Single and Simultaneous Adsorption of Cr(VI) and Cu (II) on a Novel Fe3O4/Pine Cones Gel Beads Nanocomposite: Experiments, Characterization and Isotherms Modeling

Manel Touihri, Fatma Guesmi, Chiraz Hannachi, Béchir Hamrouni, Lotfi Sellaoui, Michael Badawi, Jordi Poch, Núria Fiol

Version of Record: https://www.sciencedirect.com/science/article/pii/S1385894721006926
Manuscript_71617bbd801f7825770e8f3801bf4b7a

Single and Simultaneous adsorption of Cr(VI) and Cu (II) on a novel Fe_3O_4/pine cones gel beads nanocomposite : Experiments, Characterization and isotherms modeling

Manel Touihri[1,*], Fatma Guesmi[1], Chiraz Hannachi[1], Béchir Hamrouni[1], Lotfi Sellaoui[2], Michael Badawi[3, *], Jordi Poch[4], Núria Fiol[5, *]

[1]Laboratory of desalination and water treatment LR19ES01, Faculty of Sciences of Tunis, University of Tunis EL Manar, 2092, Tunis, Tunisia.

[2]Laboratory of Quantum and Statistical Physics, LR18ES18, Monastir University, Faculty of Sciences of Monastir, Tunisia

[3]Laboratoire de Physique et Chimie Théoriques LPCT UMR CNRS 7019, Université de Lorraine, Vandœuvre-lès-Nancy, France

[4]Applied Informatics and Mathematics Department.Universitat de Girona. Campus Montilivi, 17003, Girona, Spain.

[5]Chemical Engineering Department. Universitat de Girona. Campus Montilivi, 17003, Girona, Spain.

Corresponding authors:[*]Manel Touihri, manel.touihri@fst.utm.tn; touihri.manel1991@gmail.com

[*]Michael Badawi, michael.badawi@univ-lorraine.fr

[*]NúriaFiol, nuria.fiol@udg.edu

ABSTRACT

Recently, the use of magnetic sorbents has gained a spread attention due to their eco-friendly characteristic, ease of separation and low cost. Herein, a novel biocomposite sorbent magnetic pine cone gel beads (MPCB) was synthetized and investigated for the single and the simultaneous removal of Cu(II) and Cr(VI) from aqueous solution. Pine cones waste materials were first magnetized with Fe_3O_4 nanoparticles then were encapsulated in calcium gel beads. The physicochemical properties of the prepared MPCB were characterized via scanning electron microscopy-energy-dispersive X-ray spectroscopy (SEM-EDX), X-ray diffraction and Fourier transform infrared spectrometry (FTIR) analysis. The influences of pH, contact time and initial concentration of metal ions on the sorption process were examined. The adsorption mechanism was investigated; it mainly involved complexation/chelation with surface functional groups, electrostatic interaction and ion exchange. A physical model was adopted to attribute new physico-chemical interpretations of the adsorption mechanism. The kinetic results showed good correlation with pseudo second-order model and the equilibrium data were fitted well to the Langmuir isotherm model with maximum adsorption capacity of 68.64 and 212.22 mg g^{-1} for Cu(II) and Cr(VI) respectively. In the multi-components system, both competitive and synergistic effects were observed. An antagonism effect was exerted by Cu(II) ions on Cr(VI) sorption while Cu(II) adsorption was not affected and even slightly enhanced by the presence of Cr(V) ions. The competitive sorption behavior of metal ions was analyzed by the modified competitive Langmuir model which provides good fit for the Cu experimental data. This study proves that the MPCB hold great promise for using as effective sorbent for potentially toxic metals remediation.

Keywords

Magnetic biocomposite, potentially toxic metals, competitive adsorption, adsorption mechanism, physical modeling.

1. Introduction

With the rapid industrialization and the fast population growth, potentially toxic metal discharge from industries into environment has aroused public concern given to its hazardous effect on human health and ecological security [1-3]. Potentially toxic metals are known as chief pollutant owing to their persistence, high toxicity and non-biodegradability [4]. Their accumulation in living tissues via food chain may cause serious health and environmental problems [5]. Several diseases can be associated with chronic exposure to large amount of copper such as nausea, severe headache, liver and kidney failure, abdominal pain and neurodegenerative disorders [6, 7]. Sinkovič et al. [8] reported that an acute poisoning of 33 years old women by copper sulphate pentahydrate led to acute severe hepatic and renal failure, adrenal insufficiency and intravascular haemolysis. The copper levels in the blood reached 19.9 μmol L^{-1} when she was taken to hospital. On the other hand, chromium causes several health issues such as liver damage, kidney and respiratory damages, vomiting, severe diarrhea and allergic skin reactions [9-11]. In actual fact, chromium exists in several oxidation states in which Cr(III) and Cr(VI) are the most stable forms. Cr(VI) is highly toxic with respect to Cr(III). It is more soluble, carcinogenic and mutagenic [9]. A study by Beaumont et al. [12] reported increased stomach cancer risk in a Chinese population exposed to Cr(VI) in drinking water. These ions are mainly generated from electroplating, mining, tanneries, paint manufacture and pesticides industries [5, 13]. In this context the maximum contamination limit (MCL) on wastewater discharges were fixed to 1.3 mg Cu/L (USEPA, 2009) and 0.1 mg Cr/L (USEPA, 2009). Thus, potentially toxic metals remediation from contaminated industrial effluents prior to its discharge into environment is of utmost importance.

Various physicochemical methods have been implemented to remediate wastewater containing potentially toxic metals [14-18]. However, these techniques are associated to some

disadvantages such as high energy requirements, formation of toxics sludge and high cost [19].

Adsorption is one of the treatment technology that has proved to be an effective process for potentially toxic metal remediation because of its ease of operation, minimization of secondary waste and low cost [20]. Recently, the use of agricultural waste has been acknowledged as a promising sorbent owing to their cost-effectiveness, abundant availability and eco-friendliness [21, 22].

Several researches have been conducted to investigate the efficiency of plant materials in removing potentially toxic metals from aqueous solution [23-27]. However, using agricultural waste in their native form as adsorbents is a subject of some limitations such as leaching of plant soluble component into treated water, diffusion limitation resulting to low adsorption capacity, low specific surface area and difficulties in removal after finishing adsorption process [28-30]. To overcome these limitations, special attention was paid to the use of magnetic sorbents. The incorporation of magnetite iron oxide nanoparticles (Fe_3O_4) within agricultural waste increases the surface area and reactivity, decreases the intraparticle diffusion rate and enhances the adsorption capacity and reusability. Also, thanks to the magnetic properties of iron oxide nanoparticles the separation problem from aqueous solution can be overcame. The magnetic sorbents can be simply removed by an external magnetic field [31, 32]. Several researches have investigated the use of Fe_3O_4 nanoparticles coated biomass as adsorbent for potentially toxic metals remediation. Daneshfozoun et al. [33] reported that magnetic biosorbent based on oil palm empty fruit bunch fibers, cellulose and *Ceibapentandra* were effective for the removal of Pb(II), Co(II), Zn (II), Mn (II) and Ni (II) from aqueous solution and that the magnetic sorbents displayed 10.3% higher removal efficiency compared to raw sorbents. Zhang et al. [34] found that the adsorption capacity of Cu(II) onto magnetic chitosan microspheres immobilized *Aspergillus sydowii* (MCMAs) was

enhanced up to 119.21 (mg g^{-1}). Olive stones coated by zero-valent iron and magnetite nanoparticles were explored by Vilardi et al. [35] for Cr(VI) removal with a significant increase in adsorption capacity (2.54 and 4.11 mg Cr/g) with regard to the uncoated biomass (1.48 mg Cr/g).

In the last decade, polymeric adsorbents such as sodium alginate and chitosan have been of great interest given to their adsorption regeneration properties, good chemical stability and economic feasibility [36, 37]. Alginate was used for potentially toxic metals sorption thanks to the large number of carboxyl and hydroxyl groups capable of binding to metal ions via an ion exchange process with the crosslinking cations [38, 39]. Therefore, the development of bionanocomposites that couple the merits of agricultural waste, alginate and magnetic nanoparticles has attracted considerable interest for potentially toxic metals remediation.

As regards to the adsorption modeling, conventional models (Langmuir, Freundlich) have been adopted to interpret the adsorption equilibrium data. However, the drawn interpretations from these models provide an incomplete understanding of the adsorption mechanism. Advanced mathematical models based on statistical physics were introduced by different authors to attribute new insight of the adsorption mechanism by studying their physicochemical parameters [40].

The novelty of this research work is associated with the development, the characterization and the study of a novel magnetic biocomposite: magnetic pine cones gel beads (MPCB) for chromium (VI) and copper (II) sorption in single and multi-component system. Pine cones waste materials were first magnetized with Fe_3O_4 nanoparticles then were encapsulated in calcium gel beads. The prepared biocomposite (MPCB) was characterized using FTIR, SEM, EDX and XRD analysis. Batch experiments were conducted to investigate the adsorption behavior of MPCB gel beads towards Cr(VI) and Cu(II) in single and binary system. The effect of several parameters such as initial metal concentration, pH and contact time were also

explored. The adsorption kinetic and isotherm were studied. The competitive sorption and mechanism of metal ions onto biocomposite beads were analyzed. Multi-component sorption models were employed to analyze the equilibrium data from binary system. Finally, for a better understanding the adsorption mechanism of both ions, an advanced modeling based on physical model was applied to further explained the adsorption process.

2. Materials and Methods

2.1 Chemicals

Pine tree cones wastes were collected, washed several time with water and dried in an oven at 70°C for 24 hours. The dried waste were ground and sieved to get the desired size of particle (150 µm). Sodium alginate salt from brown algae supplied by Fluka was used as the hydrocolloidal gelling material. The $CaCl_2$ was used as fixing solution. Hydrochloric acid (HCl), hydroxide of sodium (NaOH), iron (III) chloride hexahydrate ($FeCl_3.6H_2O$), iron(II) sulfate heptahydrate ($FeSO_4.7\ H_2O$) were purchased from Scharlau. All chemicals used were of analytical grade and all the solutions used in this study were prepared using Milli-Q water (Milli-Q plus 185 systems, Millipore, Burlington, MA, USA). An appropriate amount of $K_2Cr_2O_7$ (Scharlau) and $CuCl_2{\cdot}H_2O$ (Merk) was dissolved in Milli-Q water to prepare the metal solutions.

2.2 Synthesis of iron oxide nanoparticles and Pine cones@iron oxide nanoparticles (PC@Fe_3O_4)

$PC@Fe_3O_4$ composite was prepared by in situ co-precipitation method [1]. A required amount of PC was dispersed in an iron-containing solution (400 mL), composed of $FeCl_3.6H_2O$ (7.8 g) and $FeSO_4.7H_2O$ (3.8 g) with a molar ratio of 2:1. The mixture was vigorously stirred for 10 min at 70-80 °C. Subsequently, a hydroxide sodium solution (5.0 M) was added dropwise

to the reaction system until the pH value reached 10-11 to precipitate Fe_3O_4 nanoparticles. The mixture was further kept under vigorous stirring for 1h at 80 °C and ripened for 24h at ambient temperature (20°C). The black precipitate was removed, washed severally with water and ethanol till neutral pH and dried in an oven at 70 °C for 24 h. Fe_3O_4 were similarly synthesized as aforementioned without the addition of PC powder.

2.3 Preparation of the magnetic pine cones gel beads (MPCB)

Sodium alginate (3%) was prepared by dissolving 3 g of Na-alginate in 100 mL of deionized water at 65 °C under constant stirring. The mixed solution was cooled down and a needed amount of PC@Fe_3O_4 (1g) was added with stirring. Then, it was dropped into a 0.3 M $CaCl_2$ solution and soaked in this solution for 24 h to give the sufficient rigidity. The beads were further filtered and washed with deionized water to eliminate the excess of chloride calcium. The magnetic pine cones gel beads (MPCB) were obtained. Calcium alginate beads (Blank beads BB), Pine cone beads (PCB) and iron oxide nanoparticles beads (magnetite beads MB) were similarly prepared for comparison sake. The size of prepared beads was found to be 3 mm. The produced beads were stored in deionized water in airtight plastic recipient in the fridge at 5°C for future using.

2.4 Characterization

The Fe_3O_4 nanoparticles, PC@Fe_3O_4 biocomposite and the gel beads were characterized by several techniques. Scanning electron microscopy (SEM) and energy-dispersive X-ray spectroscopy (EDX) analysis were conducted to investigate the surface morphology and the elemental analysis of the adsorbent before and after adsorption using an electron microscope Zeiss DSM 960 A equipped with energy dispersive X-ray analyser Link Isis Pentafet (Oxford). Micrographs in the Backscattered Electron mode (BSE) were also recorded to detect the presence of metallic nodules on sorbent surfaces. X-ray diffraction (XRD) spectra

were taken on a Bruker D8 QUEST ECO X-ray diffractometer with Cu-Kα radiation to investigate the crystalline structure of samples. Fourier transformed infrared spectra (Bruker Alpha) were recorded in the range 400-4000 cm^{-1} to investigate the surface functional groups before and after adsorption.

2.5 Adsorption experiments

Batch adsorption experiments were conducted in stoppered glass tubes where 40 beads of MPCB were added to 10 mL of metal single or binary mixture for different pre-treated time and pH. The mixture was vigorously stirred in a rotatory shaker (Stuart STR4) at room temperature. After the equilibrium was reached, the beads were removed by filtration. The residual concentration was measured by Flame Atomic Absorption Spectroscopy FAAS (VARIAN 22O FS). The removal efficiency R (%) and the adsorption capacity q_e (in mg g^{-1} and mg $beads^{-1}$) were evaluated using the following expression:

$$R(\%) = \frac{C_i - C_e}{C_i} \times 100 \quad (1)$$

$$q_e(mg/g) = \frac{C_i - C_e}{M} \times V \quad (2)$$

$$q_e(mg/beads) = \frac{C_i - C_e}{number\ of\ beads} \times V \quad (3)$$

where C_i and C_e (mg L^{-1}) are the initial and equilibrium concentration of metal ions. M is the adsorbent dose (g) and V is the solution volume (L).

The effect of pH was studied over the range 1-11 and it was adjusted using HCl or/and NaOH solution (0.1 mol L^{-1}). The pH was measured using a pH meter (CRISON GLP21). Adsorption isotherms were studied by varying the metal initial concentration from 10 to 3500 mg L^{-1} for Cr(VI) and from 10 to 2000 mg L^{-1} for Cu(II). The kinetic study was investigated for 48 h at constant initial concentration (250 mg L^{-1}). The sorption experiments were carried out in duplicate and the average results are presented in this study.

3. Results and discussion

3.1 Characterization

The crystal structures of PC@Fe_3O_4 biocomposite and the prepared Fe_3O_4 nanoparticles were investigated by XRD analysis as illustrated in Fig. 1. The XRD pattern (Fig. 1a) of prepared Fe_3O_4 nanoparticles exhibited six characteristic peaks at 2θ= 30.1°, 35.8°, 43.1°, 53.6°, 57° and 62.9° assigned to (220), (311), (400), (422), (511) and 440 plans relative to the cubic phase nanoparticles of Fe_3O_4 with a face-centered cubic structure (JCPDS No. 89-3854) [41].

The PC@Fe_3O_4 pattern (Fig. 1b) revealed the presence of a sharp peak at 22°, indicating the presence of amorphous carbon [42]. The main peaks of Fe_3O_4 magnetite were indexed in PC@Fe_3O_4 XRD pattern indicating that the Fe_3O_4 was successfully deposited on the surface.

The morphology and the surface feature of prepared beads were assessed by scanning electron microscopy (Fig. 2). The external shapes of prepared beads were spherical (Fig. 2a, c, e and g). The SEM images of PCB, MB and MPCB revealed a rough and heterogeneous surface respect to BB beads which has a smooth surface (Fig. 2b, d, f and h). The surface roughness plays an important role in metal ions binding since it increased the contact area, which made the surface easier for metal sorption. SEM micrographs of MB and MPCB (Fig.2d and h) revealed differences in nanoparticles distribution. Backscattered picture of MPCB showed up dots of brightness compared to the PCB backscattered picture that could indicate aggregation of magnetite, probably due to their magnetic properties. On the other hand, the extended brightness observed in the backscattered picture of MPCB seem indicate a well dispersed nanoparticles at the pinecones surface (Fig. S1 (a and b)).

The elemental analysis of prepared sorbents was investigated by EDX and the results are shown in (Fig. 3a-d). The EDX results of MPCB confirmed the deposition of Fe_3O_4

nanoparticles on pine cones surface and the main detected elements were O, C, Fe and Ca atoms (Fig. 3d).

The surface functional groups of prepared beads were examined by FTIR analysis and the spectra were presented in Fig. 4. The blank beads spectra displayed a broad band at 3286 cm^{-1} related to hydroxyl groups, the peak at 2955 cm^{-1} is attributable to CH stretching vibration, The doublet of bands at 2372-2361 cm^{-1} were assigned to the O=C=O stretching strong bending vibration of the carbon dioxide. the peaks at 1592 and 1416 cm^{-1} were associated to stretching of the carboxyl group ($-COO^-$) and the peak at 1019 cm^{-1} is identified as a characteristic peak for the -C-O-C and -C-O stretching on polysaccharide [33, 43-45]. The spectrum of MB showed a broad band at 580.71 cm^{-1} associated to Fe-O [46, 47], the peaks at 3361, 3000, 2370-2361,1600, 1424 and 1026 cm^{-1} were representative of OH groups, CH stretching vibration, O=C=O, -COOH, C=O groups and C-O-C stretching vibration respectively. FTIR spectra of pine cones beads provides evidence of the presence of hydroxyl, carboxyl, carbonyl and CH groups that appeared at 3275, 2850, 1600,1400 and 1017 cm^{-1}. By magnetizing the pine cones, a new peak appeared in the FTIR spectra of MPCB at 533 cm^{-1} attributed to Fe-O vibration. Except the Fe-O peak, the MPCB spectrum was similar to the PC spectra presenting the same surface functional groups.

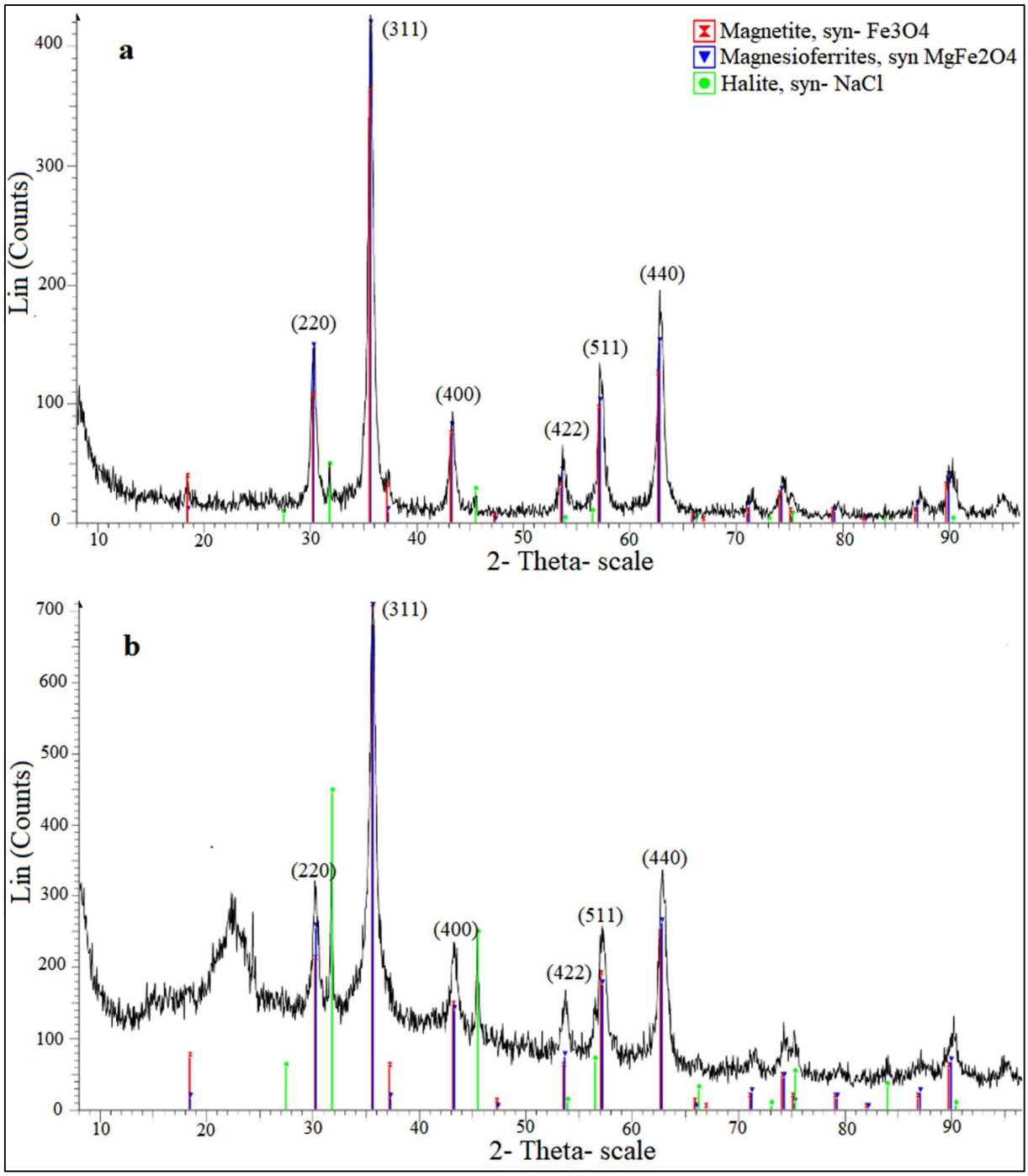

Fig.1. XRD pattern of: (a) synthesized Fe_3O_4 nanoparticles and (b) PC@Fe_3O_4 biocomposite.

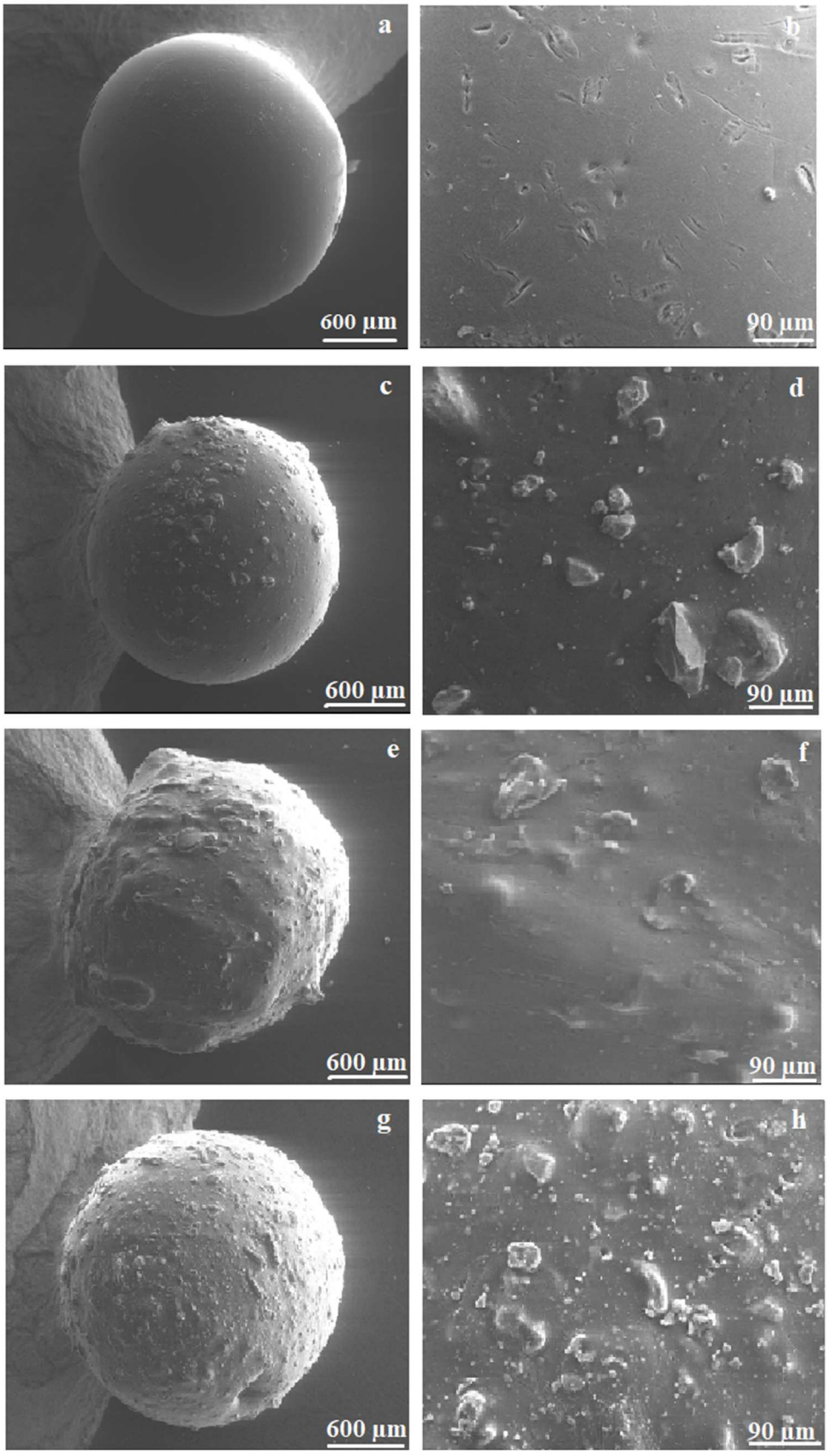

Fig.2. SEM figures of prepared sorbents: (a, b) BB, (c, d) MB, (e, f) PCB and (g, h) MPCB (magnification: 32x and 200x).

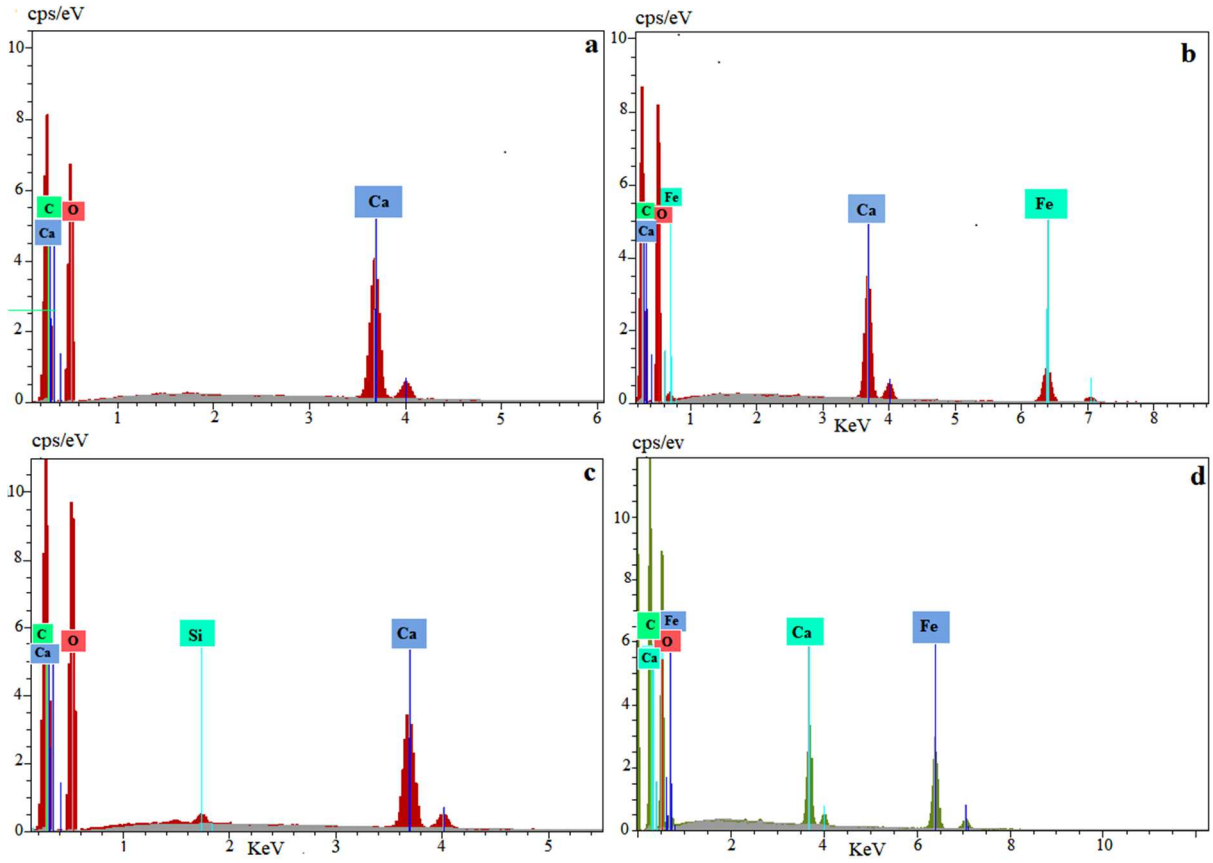

Fig. 3. EDX spectra of prepared sorbents: (a) BB, (b) MB, (c) PCB and (d) MPCB.

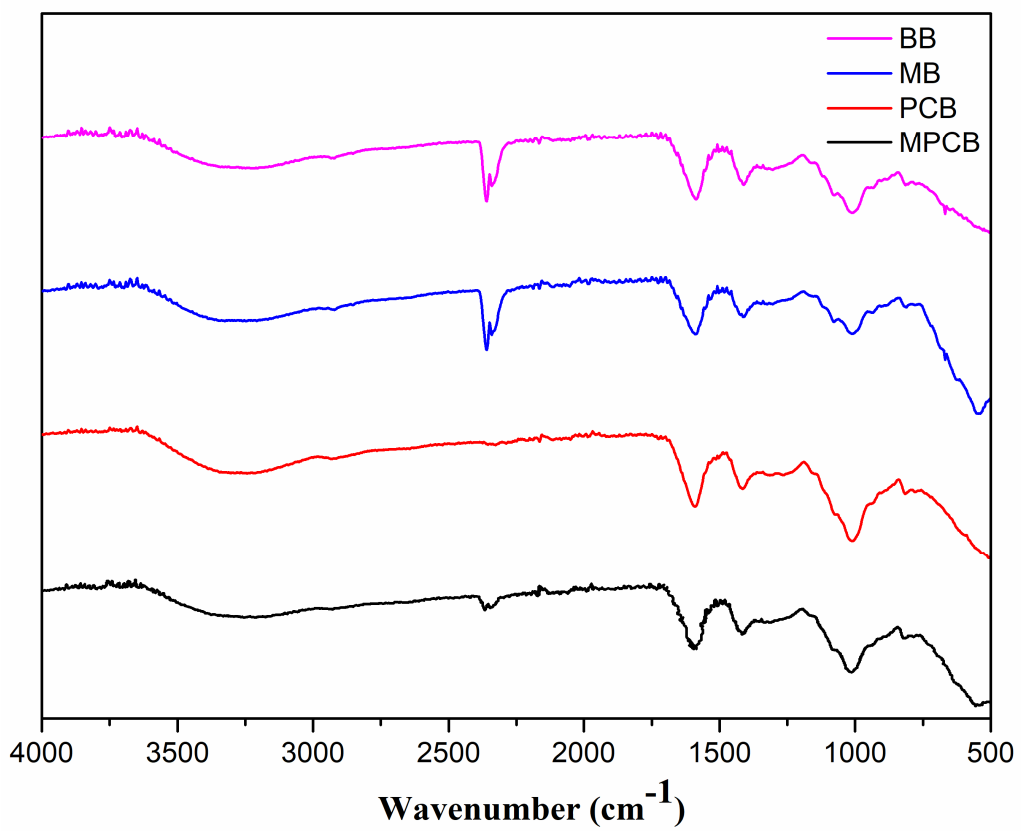

Fig.4. FTIR spectra of prepared sorbents: BB, MB, PCB and MPCB.

3.2 Effect of pH

pH solution significantly influenced the adsorption behavior since it affects both metal ion speciation and surface properties of the adsorbent. The effect of pH on the adsorption of Cr(VI) and Cu(II) onto MPCB was examined over the range 1-11 with an initial concentration of 250 mg L^{-1} and adsorbent dose of 40 beads/10 mL (Fig. 5). The results indicated that the percentage of Cu(II) removal was enhanced from 21% to 92% as the pH increased from 1.63 to 5.05, then decreased at alkaline medium. The maximum Cu(II) sorption was 23.12 mg g^{-1} at pH 5.05. Accordingly, optimum pH was fixed at 5 for Cu(II) sorption. Similar behavior was observed in the case of Cu adsorption onto BB, MB and PCB (Fig. S2). Beyond pH 6, there is a possibility of precipitation of Cu ions.

This behavior can be attributed to the fact that at a lower pH, the high concentration of hydronium ions leads to competition between H^+ and Cu(II) ions for binding sites [48]. This occurrence was associated to the presence of -COOH and –OH surface groups, at a highly acidic pH, the surface carboxylic groups are in carboxylic form (pKa values 3-5) [31], the hydronium ions will compete with the metal cations for the adsorption sites leading to lower uptake and lower removal efficiency [5]. The increase in solution alkalinity leads to the deprotonation of surface functional groups while acquiring negative charges, thus favoring the electrostatic attraction between the positively charged Cu(II) ions and the negative binding sites [1]. Indeed, the subsequent diminution of protons on the surface make more available adsorption sites for copper binding, resulting to the increased removal efficiency [49]. These results are in good agreement with previous literature data [50]. For pH higher than 6 copper (II) ions starts to precipitate as copper hydroxide, this may lead to the misinterpretation of the adsorption data. In order to avoid that the copper dioxide precipitate was dissolved and the total Cu was determined. For the higher pH, Cu (II) ions were not available to be adsorbed by the MPCB due to the spontaneous formation of copper hydroxides [30]. In the case of Cr(VI) (Fig. 5), the maximum removal efficiency of Cr(VI) was observed at pH 1.31, it reached 58 % then it decreased to reach 43 % at pH 10. The pH–dependent Cr(VI) removal behavior could be ascribed to different Cr(VI) speciation. The chromium (VI) ions mainly exist in aqueous solution as $HCrO_4^-$, $Cr_2O_7^{2-}$ and CrO_4^{2-}. $HCrO_4^-$ and $Cr_2O_7^{2-}$ are the two predominant forms over the pH range of 1-6 and above pH 6, chromate ions (CrO_4^{2-}) are the dominant chromium species [51, 52]. At low pH, the surface sorbent is highly protonated and positively charged, this lead to electrostatic attraction between these positively charged binding sites and the negative charged dichromate ions [31]. In addition the reduction of Cr(VI) to Cr(III) is favored at lower pH [53]. Fe(II) is known as a potential reducing agent that can reduce Cr(VI) to Cr(III) under acidic conditions. The iron contained in magnetite is in two oxidation states:

Fe (II) and Fe(III), the Cr(VI) will be reduced to Cr(III) by the Fe(II). Cr(III) may be adsorbed onto MPCB via surface complexation with the functional groups[31, 53, 54]. The reduction of Cr(VI) to Cr(III) occurred mainly via the following equations:

$$Cr_2O_7^{2-} + 14\ H^+ + 6\ e^- \longrightarrow 2\ Cr^{3+} + 7\ H_2O \quad (4)$$

$$HCrO_4^- + 7\ H^+ + 3\ e^- \longrightarrow Cr^{3+} + 4\ H_2O \quad (5)$$

$$HCrO_4^- + 3\ Fe^{2+} + 7\ H^+ \longrightarrow Cr^{3+} + 3\ Fe^{3+} + 4\ H_2O \quad (6)$$

$$CrO_4^{2-} + 3\ Fe^{2+} + 8\ H^+ \longrightarrow Cr^{3+} + 3\ Fe^{3+} + 4\ H_2O \quad (7)$$

To sum up, the increase in removal efficiency of Cr(VI) at lower pH was favored due to the electrostatic attraction and the Cr(VI) reduction mechanism.

As the pH increased the degree of surface protonation decreased. The large abundance of OH^- ions will compete with the negative charged chromium ions (CrO_4^{2-}) for the adsorption sites on MPCB [55]. Besides, the electrostatic repulsion between the same charged species will be accentuated (ie: adsorbate and adsorbent) [56]. Therefore, the removal efficiency decreased.

On the other hand, the increase in pH will decrease the Cr(VI) reduction and the sorption of Cr(VI) as Cr(III) will decrease. pH 2 will be selected as optimum pH for the rest of experiments.

The different prepared beads showed similar trend for the effect of pH on Cr(VI) recovery. The removal efficiency of Cr(VI) was maximized at highly acidic pH then decreased as the pH increased (Fig S2).

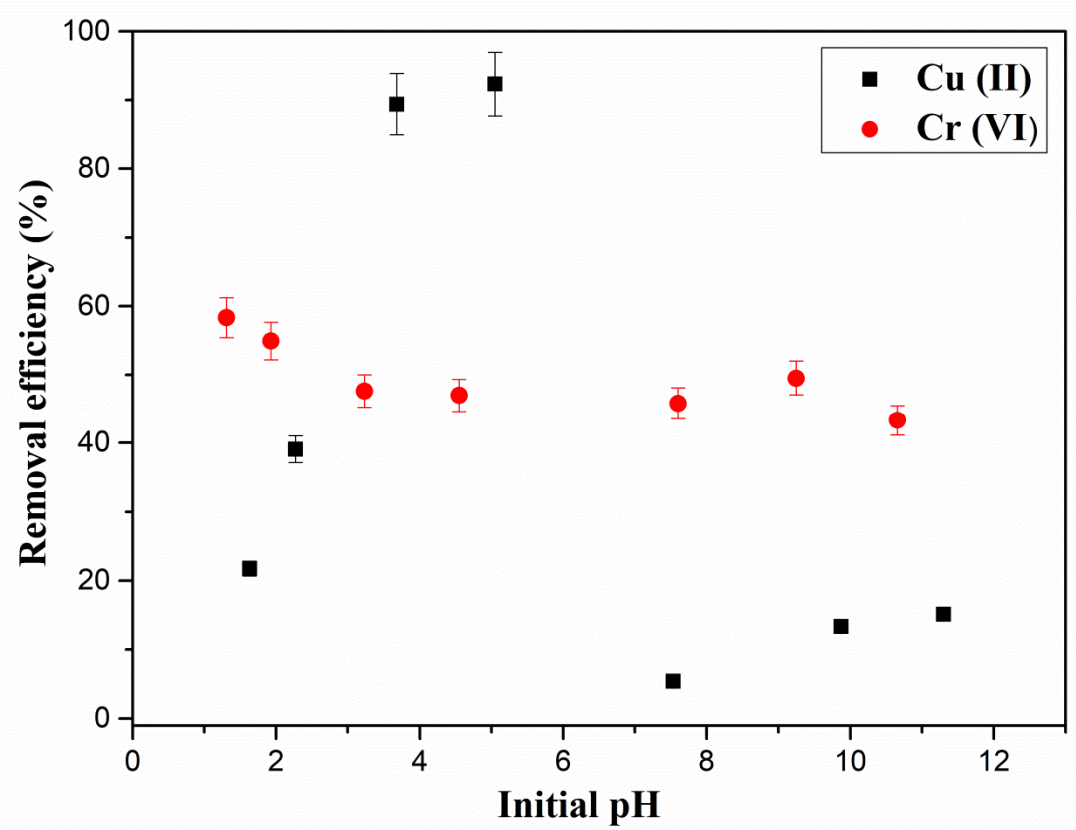

Fig. 5. (a) Effect of pH on the sorption of Cu(II) and Cr(VI) onto MPCB (initial concentration:250 mg L^{-1}).

3.3 Effect of contact time and kinetic study

3.3.1 Effect of contact time

Fig. 6 displayed the impact of contact time on Cu(II) and Cr(VI) adsorption onto MPCB at an initial concentration of 250 mg L^{-1} and an adsorbent dose of 40 beads/10 mL. As shown in the Fig. 6, the adsorption rate was fast at the beginning of experiment then it was slowed down till reaching the equilibrium. For instance, 78% of adsorption capacity of Cu(II) was attained in 30 min and the equilibrium was reached in 2 hours. In a similar way, Plohl et al. demonstrated a rapid uptake of Cu(II) ions by carboxymethyl chitosan covalently linked to silica-coated core-shell magnetic nanoparticles at the first 30 min and that the equilibrium was attained within 2 hours [30]. Similarly, more than 69% of adsorption capacity of Cr(VI) was

attained in the first 30 min of adsorption experiments and the equilibrium was reached in 2 hours. This trend could be ascribed to the abundant availability of binding sites in the first stage of experiment which subsequently became limited in the late stage of adsorption [57]. In another study, Yu et al. [58] reported a similar behavior, a rapid removal of Cr(VI) (94%) was attained at the first 2 hours followed by a nearly total removal after 12 hours of contact time.

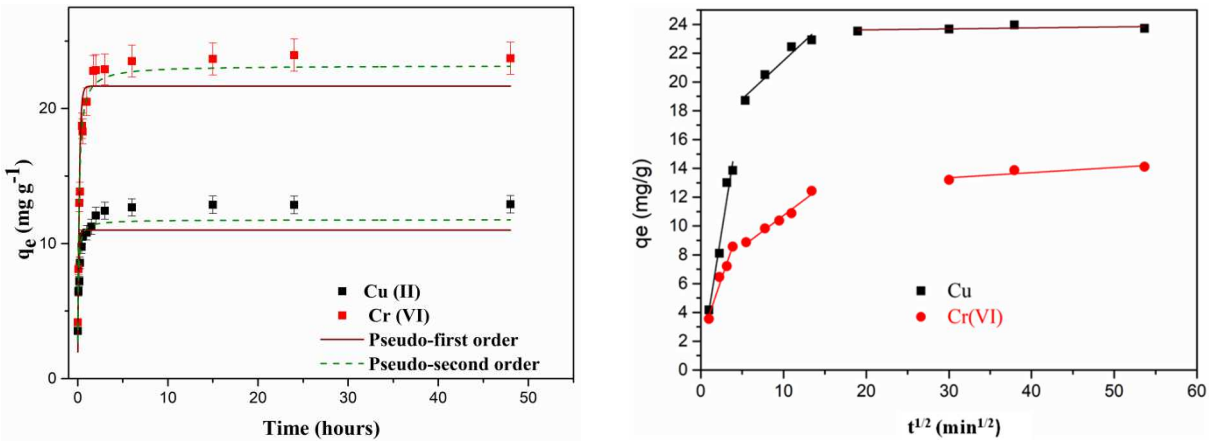

Fig. 6 (a) Effect of contact time/fitting curves of pseudo-first order and pseudo-second order models, (b) intra-particle diffusion model for the sorption of Cu(II) and Cr(VI) onto MPCB (initial concentration:250 mg L^{-1}).

3.3.2 Kinetic study

The adsorption kinetic study is a significant tool for analyzing the adsorption process. It provides valuable experimental information for designing water treatment system. The kinetic experimental data of Cu(II) and Cr(VI) sorption onto MPCB were fitted to the kinetic models: pseudo-first-order, pseudo-second-order and Weber-Morris models ((Fig. 6a and b)) to investigate the sorption mechanism.

The pseudo-first-order model was suggested by Lagergren [59]. This model describes the adsorption in solid/liquid system and can be defined as follow:

$$q_t = q_e(1 - e^{-k_1 t})(8)$$

Where q_e and q_t are the adsorption capacities (mg g^{-1}) at equilibrium and at time t(min), $k_1(min^{-1})$ is the equilibrium rate constant for pseudo first-order model.

The pseudo second-order model is given by the equation (9) [60]

$$q_t = \frac{k_2 q_e^2 t}{1+k_2 q_e t} \quad (9)$$

Where k_2 (g mg^{-1} min^{-1}) is the rate constant for pseudo second-order model. This model suggests the kinetic behavior of chemisorption as a rate limiting step.

The Weber-Morris model is applied to determine the rate controlling step in the adsorption process [61] and it can be defined as follows:

$$q_t = k_{id} t^{1/2} + C \quad (10)$$

where k_{id} (mg g^{-1} $min^{-1/2}$) is the intra particle diffusion rate constant, $t^{1/2}$ ($min^{1/2}$) is the square root of time, C (mg g^{-1}) is the intercept value. The C value informs about the boundary layer effect, a large value of intercept indicates an important boundary layer effect. If the plot q_t versus $t^{1/2}$ is linear and passes through the origin then the intraparticle diffusion is the rate-determining step in the adsorption process [62].

The kinetic models' parameters were listed in Table 1. The coefficient correlation values R^2 of pseudo-second-order model are higher and much closer to unity compared to those found with the pseudo-first-order model for both metals. Additionally, the q_e calculated from the pseudo-second-order model are in good agreement with the experimental values (For Cu(II): $q_{e,cal}$= 24.09 mg g^{-1} $q_{e,exp}$= 23.87 mg g^{-1}; for Cr(VI): $q_{e,cal}$: 12,60mg $g^{-1}$$q_{e,exp}$: 12.92 mg g^{-1}). These finding indicate that the pseudo-second-order model describes well the adsorption of

Cu(II) and Cr(VI) onto MPCB. This model suggests that the chemisorption involving sharing or electron exchange between metal ions with adsorbent is the rate limiting step [21, 63].

The Weber-Morris model was applied to examine the rate determining step in the adsorption process. The plot q_t versus $t^{1/2}$ is illustrated in Fig. 6b. The multi-linearity of the plot suggests that the adsorption process of Cu(II) and Cr(VI) took place in multi-steps. The first step was related to the external film diffusion, the intra-particle diffusion was indicated as the second step and the third step corresponds to the final equilibrium. The results showed that the linear curves doesn't pass through the origin, implying that the intra-particle diffusion was not the sole governing step but more the one mechanism is involved in the adsorption process [64].

Table 1 kinetic model parameters for the adsorption of Cu(II) and Cr(VI) ions onto MPCB.

Kinetic models	**Parameters**	**Metal ions**	
		Cu(II)	**Cr(VI)**
Pseudo first order	q_e (mg g^{-1})	22.85	12.04
	k_1 (min^{-1})	0.068	0.098
	R^2	0.949	0.832
	χ^2	2.11	1.40
Pseudo second order	q_e (mg g^{-1})	24.09	12.60
	k_2 (g mg^{-1} min^{-1})	0.004	0.013
	R^2	0.987	0.947
	χ^2	0.52	0.46
Intra-particle diffusion	C (mg g^{-1})	16.16	6.40
	K_{id} (mg $L^{-1/2}min^{-1/2}$)	0.532	0.434
	R^2	0.933	0.971

3.4 Equilibrium study on single metal system

3.4.1 Adsorption isotherms and experimental results modeling

Adsorption isotherms are widely applied to describe the adsorption behavior. Langmuir and Freundlich isotherms are the most common one. Langmuir model presumes that the adsorption occurs on a homogeneous surface and that all binding sites have similar energy and similar affinity for each adsorbate, suggesting the monolayer sorption behavior [65]. The non-linear form of Langmuir model is expressed in equation 11:

$$q_e = \frac{q_{max} K_L C_e}{1 + b C_e} \quad (11)$$

Where q_e is the adsorption capacity at the equilibrium (mg g^{-1}), K_L is the Langmuir constant related to the energy of sorption, q_{max} is the maximum sorption capacity (mg g^{-1}) and C_e is the metal concentration in the liquid phase at the equilibrium (mg L^{-1}).

The Langmuir model is characterized by a dimensionless parameter R_L (Eq. (12)) called separation factor indicates either the adsorption is unfavorable ($R_L > 1$), Linear ($R_L = 1$), favorable ($0 < R_L < 1$) or irreversible ($R_L = 0$).

$$R_L = \frac{1}{1 + K_L c_0} \quad (12)$$

where K_L is the Langmuir constant and C_0 is the initial metal concentration (mg L^{-1}).

Freundlich isotherm is an empirical model based on heterogeneous multi-layer adsorption [65]. The Freundlich model is given in equation 13:

$$q_e = K_F C_e^{1/n} \quad (13)$$

where K_F is the Freundlich constant related to adsorption capacity and n is the adsorption intensity.

The effect of initial concentration on Cu(II) and Cr(VI) sorption onto MPCB was investigated over the range of 10-2000 mg L^{-1} and 10-3500 mg L^{-1} respectively, at an

optimum pH and time and the equilibrium data was fitted to Langmuir and Freundlich isotherms. The results are exhibited in Fig. 7 and the calculated parameters are gathered in Table 2. The best fit of an adsorption system is evaluated by the coefficient of correlation R^2 and the nonlinear chi-square test χ^2. The closer coefficient correlation to 1 and the smaller χ^2 value indicated the good fit of the isotherm model [66].

As presented in Table 2, Langmuir model provides a higher coefficient correlation R^2 with a lower χ^2(Cu(II) :R^2: 0.975, χ^2: 13.55; Cr(VI): R^2: 0.989, χ^2: 22.65) for Cu(II) and Cr(VI) respectively with respect to Freundlich model (Cu(II) :R^2: 0.936, χ^2: 35.18; Cr(VI): R^2: 0.985, χ^2: 33.75), indicating that the Langmuir isotherm describes well the adsorption of the two metal ions onto MPCB. This model indicates the monolayer sorption without interaction between analytes molecules. The maximum adsorption capacity obtained with Langmuir model were 68.64 and 212.22 mg g^{-1} for Cu(II) and Cr(VI) respectively. R_L values ($R_{L,Cu}$: 0.17; $R_{L,Cr(VI)}$ 0.83) ranging between 0 and 1 for both metals indicate that the adsorption was favorable. This result was confirmed by the n_F values of the Freundlich model which were ranging between 1 and 10.

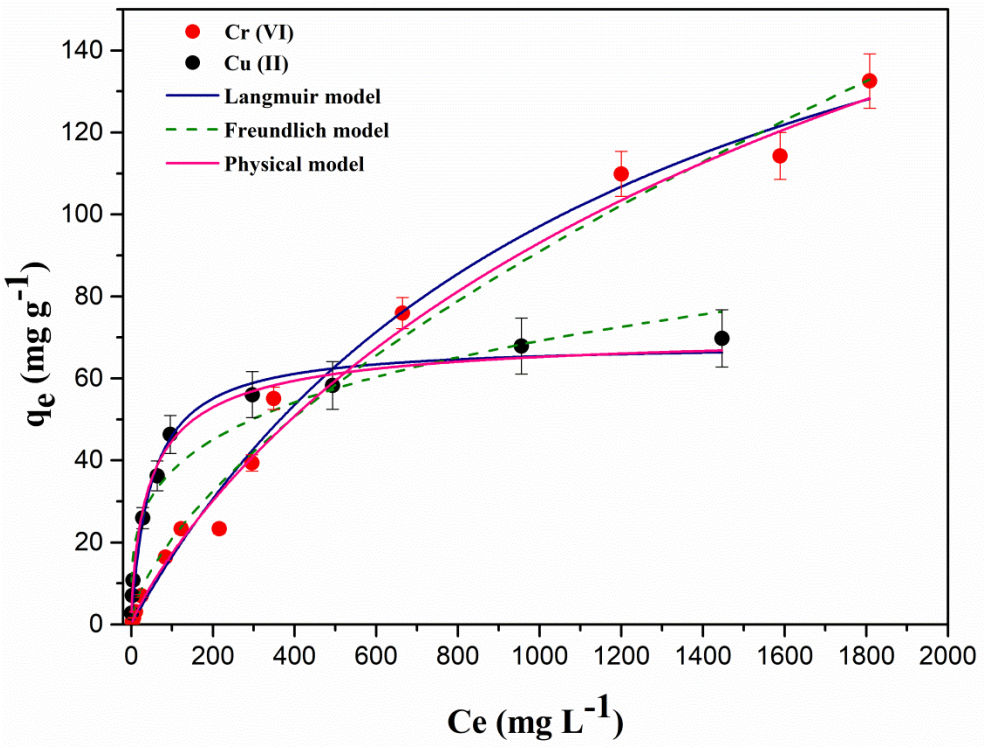

Fig. 7. Fitting curves of Langmuir, Freundlich, and the physical isotherm model.

Table 2 Adsorption isotherms constants of the adsorption of Cu(II) and Cr(VI) ions onto MPCB.

Isotherm models	**Parameters**	**Toxic metals**	
		Cu (II)	**Cr (VI)**
Langmuir	K_L (L mg^{-1})	0.020	8.44E-04
	q_{max}(mg g^{-1})	68.64	212.22
	R^2	0.975	0.989
	χ^2	13.55	22.65
Freundlich	K_F ($mg^{(1-1/n)} L^{1/n} g^{-1}$)	11.90	1.11
	n	3.94	1.56
	R^2	0.936	0.985
	χ^2	35.18	33.75
Physical model	n	0.67	0.97
	D_m	116.11	231.12

	$C_{1/2}$ (mg L^{-1})	72.40	1325.60
	R^2	0.994	0.989
	χ^2	4.07	24.82

In order to explore the influence of magnetization and encapsulation on the adsorption process, the adsorption performance of prepared beads (i.e: blank beads, magnetite beads, pine cones beads, and magnetic pine cones beads) in removing Cr(VI) and Cu(II) at an initial concentration of 250 mg L^{-1} was compared (Fig. 8). In General, the MPCB showed a significant increase in the adsorption capacity of Cr(VI) and Cu(II) ($q_{e,exp(Cu(II))}$: 69.77 mg g^{-1} $q_{e,exp(Cr(VI))}$: 132.52 mg g^{-1}) compared to raw material ($q_{e,exp(Cu(II))}$: 27.11 mg g^{-1} $q_{e,exp(Cr(VI))}$: 27.64 mg g^{-1}). As exhibited in Fig.8, MPCB showed an enhancement in the adsorption capacity of Cr(VI) after loading magnetite on PC surface compared to PCB beads. The increase may be due to sorption properties of magnetite. By loading the magnetite on pine cones surface, more binding sites will be provided and the Fe(II) in the magnetite may reduce Cr(VI) to Cr(III) which facilitate its adsorption on MPCB surface. Magnetite beads showed a good adsorption $q_{e(Cr)}$: 0.0216 mg/beads for Cr(VI) at initial 250 mg/L Cr(VI) concentration meanwhile the blank beads showed a relatively lower one $qe_{(Cr)}$: 0.020(mg/beads) at the same initial concentration.

In the case of copper, the adsorption capacity has not significantly changed compared to those obtained with the blank and magnetic pine cones beads. This is explained by the main ion exchange process with Ca(II) ions of the gel. This was confirmed by the EDX results (fig S3), in which a decrease of calcium percentage after Cu(II) ions sorption was observed.

It is noteworthy that by encapsulating the raw materials in calcium alginate beads, the PCB exhibited a higher adsorption capacity for Cr(VI) and Cu(II) (($q_{e(Cr)}$:14.28 mg/g; $q_{e(Cu)}$: 23.25 mg/g, both at initial concentration 250 mg/L) compared to the raw materials (q_{eCr}:11.2 mg/g; q_{eCu}: 21.5 mg/g) at the same initial concentration, which indicates that the alginate

significantly contribute in the adsorption process. Thus, the encapsulation of the raw material has enhanced its removal efficiency.

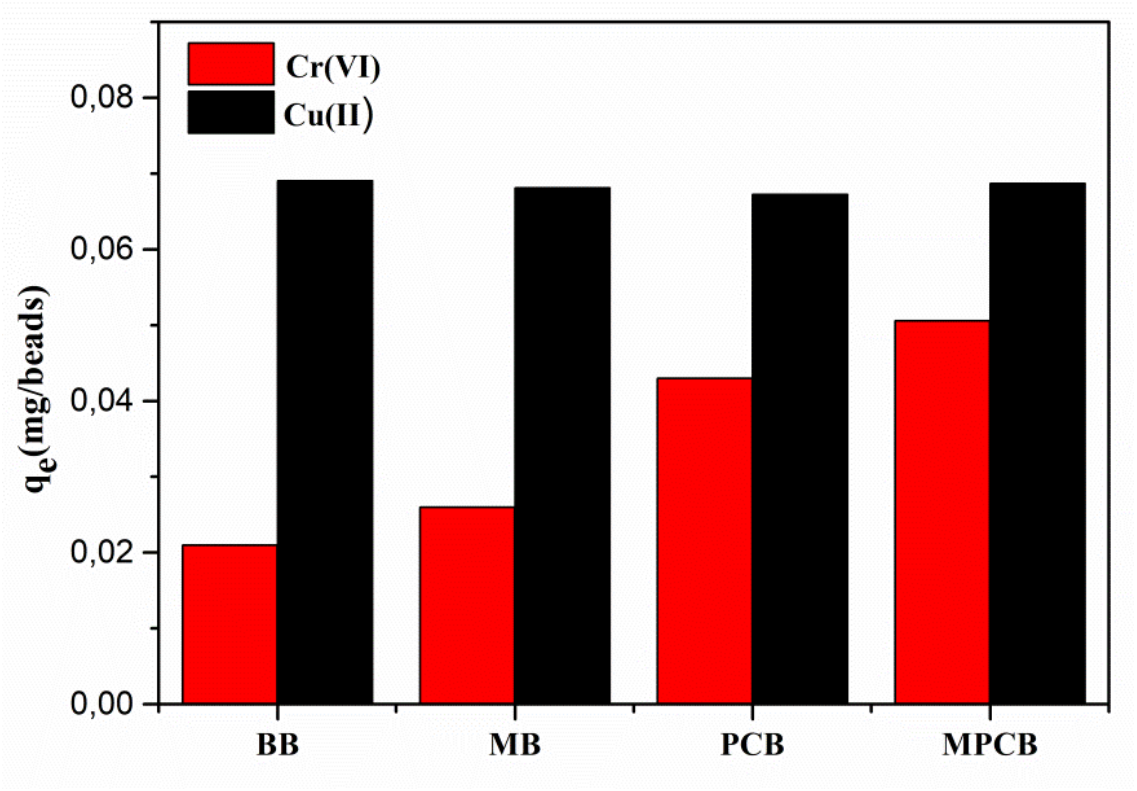

Fig. 8. Comparison of adsorption capacities of prepared sorbents (BB, MB, PCB, MPCB) towards Cu(II) and Cr(VI) for fixed initial concentration (250 mg L^{-1}).

The isotherm modeling results of Cr(VI) and Cu(II) sorption onto BB, MB and MPCB (Fig S4, table S1) demonstrated that the Langmuir model is suitable for describing the adsorption behavior since it provided the highest coefficient correlation R^2 with the lowest χ^2, suggesting the monolayer sorption.

The experimental maximum sorption capacity of Cr(VI) and Cu(II) by the prepared beads was determined. The MPCB showed the highest adsorption capacity for Cr(VI) (q_{max}: 132.52 mg g^{-1}) followed by the PCB (q_{max}: 130.66 mg g^{-1}), then the MB (q_{max}: 130.25 mg g^{-1}) and the lowest value of adsorption capacity corresponded to the BB (q_{max}:112.53 mg g^{-1}). In the case

of Cu(II), BB exhibited a high adsorption capacity (q_{max}: 176.13 mg g^{-1}) followed by MB (q_{max}: 114.69 mg g^{-1}), PCB (q_{max}: 84.80 mg g^{-1}) and MPCB (q_{max}: 69.77 mg g^{-1}).

3.4.2 Theoretical interpretation of the adsorption mechanism via a physical model

An advanced physical model is able to attribute new theoretical insights of the adsorption mechanism of both tested ions on MPCB. Based on this model, it was considered that the adsorption process can be performed via a formation of one adsorbed layer (Langmuir hypothesis). It was assumed also that the leading adsorption functional group can accept one (Langmuir hypothesis), a fraction of ion or more than one ion. The expression of this model is described by Eq.(14) [67]:

$$q_e = \frac{n\, D_m}{1+(\frac{C_{1/2}}{C_e})^n} \quad (14)$$

where n is defined as the number of the ions per leading adsorption function group (adsorption site), D_m represents the density of leading adsorption sites at saturation, and $C_{1/2}$ is the concentration at half-saturation. The fitting of the experimental adsorption data is illustrated in Fig. 7. As can be seen from Fig. 7, a good correlation between this model and the data was observed, considering an uncertainty around 3% for our computed values of n. The values of the determination coefficient R^2 are 0.989 and 0.995 for Cr(VI) and Cu(II) adsorption respectively. Fitting results provided that the n (Cr(VI))-adsorbent and n (Cu)-adsorbent values were 0.96 and 0.67 respectively. This theoretical evidence demonstrated that the leading adsorption functional group accepted 0.96 ions of Cr(VI) and 0.67 ions of Cu(II). Referring to the literature, it was discussed that [67]:

If $n < 0.5$, the ions can be interacted via two or more adsorption sites (multi-interaction process).

If n > 1, one functional group can be involved in the adsorption (multi-ionic process).

If 0.5 <n <1, the ions can be interacted via one and two functional group but with two different percentages.

Overall, we can understand that both ions were interacted during the adsorption via one and two adsorption sites but with two different percentages. For instance, considering the following equation since 0.5 < 0.96 <1:

$$0.96 = 1.x + (1-x).0.5 \quad (15)$$

where x is the percentage of adsorption via one adsorption site and 1-x is the percentage of the adsorption of Cr(VI) via two adsorption sites. Based on the calculation of this equation, it was deduced that 92% of the Cr(VI) was adsorbed via one adsorption site, and 8% via two adsorption sites. It can be concluded that the interaction via one adsorption site is very dominant. It was noted also that n (Cr(VI))-adsorbent > n (Cu)-adsorbent. This result is due to the high adsorption capacity that was demonstrated by the Langmuir model.

In the case of Cu(II), the n value was 0.67, indicating that copper ions can be interacted via one and two functional group but with two different percentages. By considering the following equation:

$$0.67 = 1.y+ (1-y).0.5 \quad (16)$$

where y is the percentage of an interaction with one functional group, and 1-y corresponds to an interaction with two functional groups.

34% of Cu(II) interacts with one adsorption site, and 66% with two adsorption sites. Overall, we can understand that the Cu ion mainly interacts with the alginate matrix by two carboxylate groups.

3.4.3 Comparison of the adsorption performance of MPCB with literature report

The maximum adsorption capacities of MPCB for the removal of Cu(II) and Cr(VI) were compared with those obtained with previously studied sorbent (Table 3). As can be seen from the Table 3, MPCB demonstrated high adsorption capacities compared with other composite adsorbents suggesting that MPCB showed a good adsorption performance toward Cu(II) and Cr(VI) ions.

Table 3. Adsorption capacities of other sorbents for C(VI) and Cu(II)

Adsorbent	qm (mg/g)		Conditions	References
	Cr(VI)	Cu(II)		
Sepiolite-supportes magnetite nanoparticles (SSMNPs)	33.4	-	pH 3, 20°C	[58]
Fe2O3-chitosan-cherry kernel shell pyrolytic charcoal composite	47.58	-	pH 2,	[68]
Graphene oxide functionalized chitosan-magnetite nanocomposite	142.85	-	pH 3	[69]
Magnetic pinecone beads	132.52	-	pH 2, 20°c	This study
Poly (methyl methacrylate)-grafted alginate/Fe3O4 nanocomposite	-	35.7	pH5, 50°C	[70]
carboxymethyl chitosan (CMC)/sodium alginate/ grapheme oxide@Fe3O4	-	55.96	pH 5, 30°C	[71]
Nanochitosan/sodium alginate/microcrystalline cellulose beads	-	43.3	pH 5	[72]
Magnetic pine cones beads		69.77	pH 5	This study

3.5 Equilibrium study on binary metal system

3.5.1 Competitive sorption of metal ions onto MPCB

The competitive adsorption of Cu(II) and Cr(VI) onto MPCB were examined by varying the initial concentration from 50 to 2000 mg $L^{-1}$for Cu(II) and from 50 to 1200 mg L^{-1} for Cr(VI). The pH was fixed at 3 for all experiments, and the results were gathered in Table 4.

As illustrated in Table 4, Cr(VI) uptake was suppressed by the coexistence of Cu(II), meanwhile Cu(II) sorption was not significantly affected by the presence of Cr(VI).

For a fixed concentration of Cu(II), the adsorption capacity of Cr(VI)was enhanced with the increase of initial concentration of Cr(VI) from 50 to 1200 mg L^{-1}. Compared to the single system, the adsorption capacity of Cr(VI) decreased in almost cases. For instance, it was reduced by 28% with Cu(II) varying from 0 to 2000 mg $L^{-1}$when operating at a fixed concentration of Cr(VI) of 750 mg L^{-1}. The reduction in adsorption capacity could be ascribed to the availability of binding sites in which metal ions are competing on and to the affinity strength [73, 74]. At acidic pH, Cr(VI) is reduced to Cr(III) and may be adsorbed in its trivalent ions. Metal ions (Cr(III) and Cu(II)) will be competing for the active sites which leads to the decrease of Cr(VI) sorption in the binary system [75, 76].

However, the q_e values for Cu(II) were enhanced in comparison with those in single system by varying Cr(VI) concentration from 50 to 1200 mg L^{-1}. For a fixed concentration of Cu(II) (2000 mg L^{-1}), the q_e of Cu(II) was enhanced by 14% with Cr(VI) varying from 0 to 1200 mg L^{-1}.

The competitive adsorption relationship in binary system could be evaluated by the ratio of sorption capacities (Rq_i) of a metal ion (i) in the presence of another metal ion (j) and in single system at the same operating conditions ($q_{e,imixture}/q_{e,isingle}$) [77, 78]. Three types of effect were identified based on Rq_i values: if $Rq_i>1$ there is a synergistic effect and the adsorption of metal ion i was favored by the coexistence of the other metal j, if $Rq_i<1$ there is an antagonist effect and the adsorption of metal ion i was inhibited by the presence of metal ion j and if $Rq_i=1$ there is no interaction [79]. The Rq_i values are listed in Table 4.The

$Rq_{Cr(VI)}$values were ranging between 0 and 1, indicating the antagonism effect exerted on Cr(VI) sorption by the coexistence of Cu(II). It can be noted also that the $Rq_{Cr(VI)}$ values increased by varying Cu(II) from 50 to 2000 mg $L^{-1}$and get closer to unity, indicating that the antagonism effect was decreased. For a fixed concentration of Cu(II), the increment of initial concentration of Cr(VI) decreased the sorption capacity ratio ($Rq_{Cr(VI)}$). These results indicate that the inhibition effect was highly influenced by Cu(II) and Cr(VI) initial concentration. At low Cu(II) concentration (i.e, 50 and 100 mg L^{-1}), the sorption capacity ratio of Cr(VI) was lower compared to higher Cu(II) concentration, revealing that the competitive behavior between Cr(VI) and Cu(II) was much stronger at low concentrations. For fixed concentration of Cr(VI) (i.e, 50 and 100 mg L^{-1}) and by varying the Cu(II) from 500 to 2000 mg L^{-1} the Rq values were equal or slightly higher to 1 indicating the non-significance of antagonist or synergetic effect. Regarding copper, the impact of coexistence of Cr(VI) on the competitive sorption of Cu(II) was insignificant considering that $Rq_{Cu(II)} \rightarrow 1$ for almost experiments. $Rq_{Cu(II)}$ values were increased as result of increasing the Cr(VI) concentration from 50 to 1200 mg L^{-1}. The presence of Cr(VI) may slightly increases the Cu(II) sorption by exerting a synergistic effect. The synergistic effect could be explained by different mechanism that may occurred in the sorption process: the reduction of Cr(VI) to Cr(III) lead to pH increase due to protons consumption, as the pH increased Cu(II) sorption was favored owing to the electrostatic attraction with the negatively charged surface, also more active sites were provided by the oxidation of several functional groups [75, 80, 81]. Additionally, the increase of anionic Cr(VI) concentration established an effective electrostatic shield against the repulsive forces between Cu(II) cations particularly from those in adjacent sites, thus increasing the amount of active sites for Cu(II) sorption [81, 82].

Table 4 Multicomponent adsorption capacities of Cu(II) and Cr(VI) in binary system using MPCB as adsorbent for fixed pH and Temperature (pH:3; T:20°C).

Binary system Cr(VI)-Cu(II)	**$C_{e,Cr(VI)}$ (mg L^{-1})**	**$q_{e,Cr(VI)}$ (mg g^{-1})**	**$Rq_{Cr(VI)}$**	**Binary system Cu(II)-Cr(VI)**	**$C_{e,Cu(II)}$ (mg L^{-1})**	**$q_{e,Cu(II)}$ (mg g^{-1})**	**$Rq_{Cu(II)}$**
50-0	10.09	4.27	-	50-0	6.49	4.31	-
100-0	50.03	5.36	-	100-0	19.54	8.33	-
500-0	333.20	21.79	-	500-0	171.09	32.28	-
750-0	558.30	23.65	-	1000-0	515.3	51.5	-
1200-0	854.60	37.62	-	2000-0	1218.4	69.77	-
50-50	12.69	3.77	0.88	50-50	10.33	4.49	1.03
100-50	50.50	4.81	0.90	100-50	22.87	8.34	1.00
500-50	311.00	13.42	0.62	500-50	175.50	34.92	1.08
750-50	516.3	11.45	0.48	1000-50	554.55	49.84	0.97
1200-50	929.20	25.50	0.68	2000-50	1396.10	77.05	1.10
50-100	14.17	3.67	0.86	50-100	11.31	4.43	1.03
100-100	55.89	4.46	0.83	100-100	20.63	8.62	1.03
500-100	329.4	13.18	0.60	500-100	197.76	33.25	1.03
750-100	521.5	10.78	0.46	1000-100	534.80	49.47	0.96
1200-100	937.20	24.25	0.64	2000-100	1451.00	69.20	0.99
50-500	14.03	4.38	1.03	50-500	4.69	4.32	1.00
100-500	55.69	5.71	1.07	100-500	13.24	8.10	0.97
500-500	394.3	9.31	0.42	500-500	141.80	29.22	0.91
750-500	564	16.36	0.69	1000-500	444.70	47.75	0.93
1200-500	935.1	25.24	0.67	2000-500	1255.0	64.62	0.93
50-1000	14.09	4.35	1.02	50-750	4.07	4.71	1.09
100-1000	57.33	5.94	1.11	100-750	10.26	8.69	1.04
500-1000	432.50	15.12	0.69	500-750	116.55	36.34	1.13
750-1000	585.00	16.26	0.69	1000-750	425.7	52.95	1.03
1200-1000	973.60	32.28	0.86	2000-750	1240.6	74.79	1.07
50-2000	14.05	4.29	1.01	50-1200	3.86	4.59	1.06
100-2000	55.07	6.18	1.15	100-1200	10.38	8.51	1.02
500-2000	510.10	17.46	0.80	500-1200	117.6	34.55	1.07

750-2000	708.40	15.99	0.68	1000-1200	379.2	56.61	1.11
1200-2000	797.00	34.91	0.93	2000-1200	1125.1	80.12	1.15

3.5.2 Multi-component isotherm modeling

A multi-component isotherm models were employed for describing the competitive metals sorption. The Langmuir sorption isotherm is commonly used in single as well as multi-component adsorption due to its performance in describing the adsorption behavior. The Langmuir mono-element sorption isotherm can be extended to multi-metals isotherm: extended, non-modified and modified competitive Langmuir models [83].

The non-modified and the extended Langmuir models are based on the assumption of the similarity of all active sites on the surface sorbent and that all sorbate molecules compete equally for the active sites. q_{max} and $K_{L,I}$ are the non-modified Langmuir model parameters derived from the mono-element Langmuir isotherm. Extended Langmuir isotherm is characterized by specific adjustable parameters for the competing metals ($q_{m,i}$ and $K_{L,i}$) [84].

In the modified competitive Langmuir model, $n_{L,i}$ a corrector parameter was incorporated to describe the interactive effect between different sorbate in solution. This parameter is characteristic of metal ions and is dependent on the other components' concentration [19].

These multi-component isotherm models are described below:

Extended Langmuir model

$$q_e = \frac{q_{max,i} K_{L,i} C_{e,i}}{1+\sum_{j=1}^{N} K_{e,j} C_{e,j}} \quad (17)$$

Non-modified competitive Langmuir model

$$q_e = \frac{q_{m,i} K_{L,i} C_{e,i}}{1+\sum_{j=1}^{N} K_{e,j} C_{e,j}} \quad (18)$$

Modified competitive Langmuir model

$$q_{e,i} = \frac{q_{m,i} K_{L,i} (C_{e,i}/n)}{1+\sum_{j=1}^{N} K_{L,j} (C_{e,j}/n)} \quad (19)$$

To evaluate the competitive effect of Cu(II) and Cr(VI) sorption onto MPCB in binary system, the equilibrium data were modeled by the modified competitive Langmuir multi-component isotherm. The estimated parameters and SSR (Eq. (20)) values were listed in Table 5.

$$SSR = \sum_{i=1}^{N} (q_{1,i,exp} - q_{1,i,cal})^2 - (q_{2,i,exp} - q_{2,i,cal})^2 \quad (20)$$

In this model, two new constant n_1 and $n_2$are incorporated as interactions factors. These parameters take into consideration the deviations from the non-modified extended Langmuir model and its assumptions [19].

3D plots of metal uptake (i.e, $q_{e,\,Cr(VI)}$, $q_{e,\,Cu(II)}$) versus the equilibrium concentration of target metal ion in the bicomponent system Cr(VI)-Cu(II) were shown in Fig. 9a and b. The curve of total metal uptake ($q_{e,Cu(II)}+q_{e,Cr(V)}$) versus of the equilibrium concentration of the two metals was exhibited in Fig. 8c. As can be seen, the 3D plot of total metal uptake has the same tend to that of Cu(II). As shown in Fig. 8a and c, the equilibrium data for copper and total metal uptake were well situated on the sorption surface isotherm meanwhile, Cr(VI) experimental data showed a slight deviations from the sorption isotherm surface (Fig. 8b). These results assume that competitive Langmuir isotherm model is suitable for describing the adsorption behavior of Cu(II) in binary metal system however, this model provides a poor fit for Cr(VI) experimental data in binary mixture.

To further examine the model performance, the predicted q_e values were plotted versus the experimental q_e values of Cu(II) and Cr(VI) in the binary system (Fig. 10 a, b and c). The q_e values were distributed around the square diagonal, the good fitting of the model is suggested by a near zero intercept and a close unity slope. The coefficient correlation R^2 for copper and total metal uptake were higher than 0.9, confirming that the competitive Langmuir model

demonstrates a good fit to the equilibrium data of Cu(II) from the binary mixture. However, R^2 value for Cr(VI) was lower than 0.9 which indicate that the competitive Langmuir model couldn't fully describe the Cr(VI) adsorption behavior.

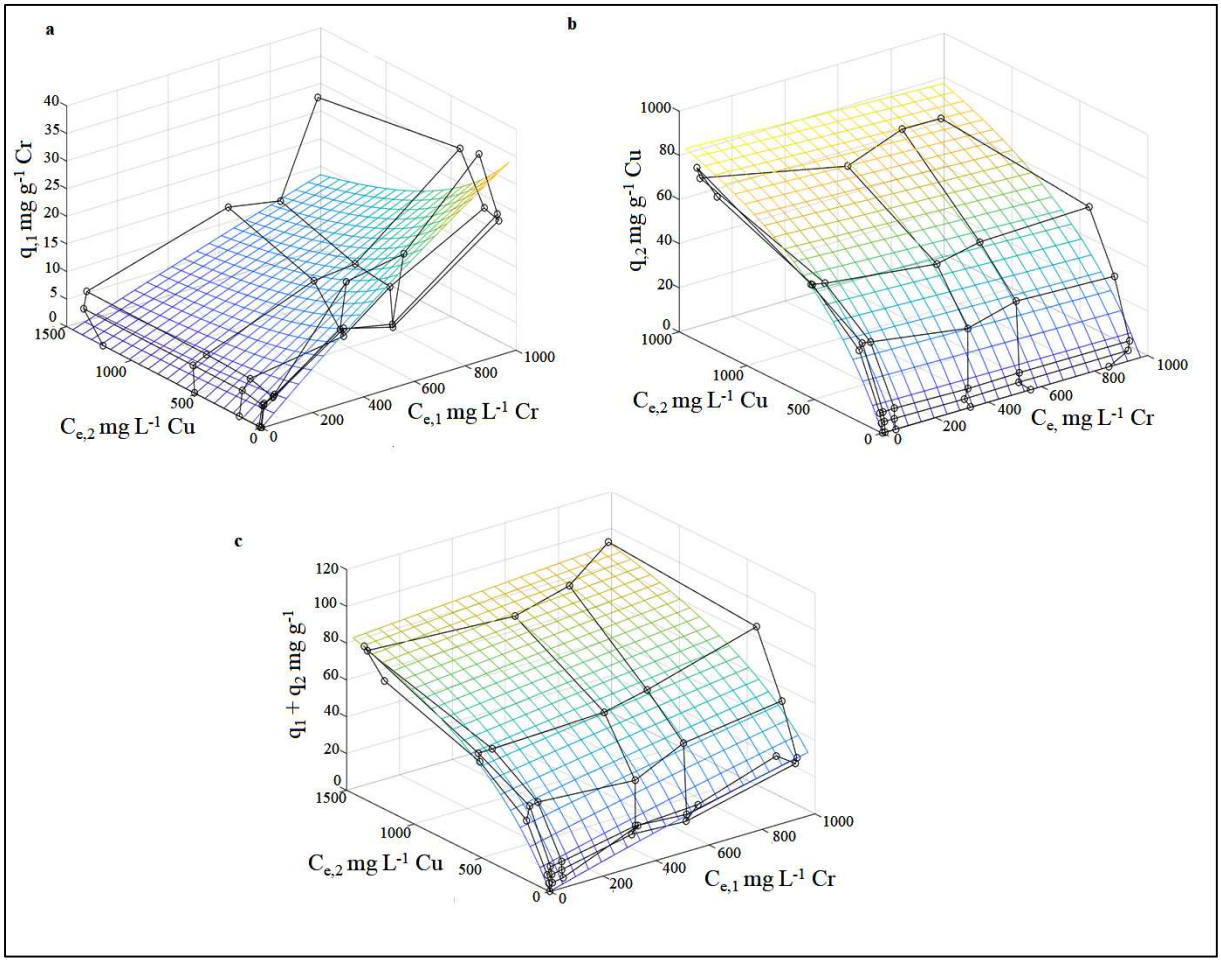

Fig. 9. Equilibrium sorption surface for: (a) Cr(VI) , (b) Cu(II) and (c) total metals uptake in binary mixture Cr(VI)–Cu(II) uptake. The surfaces are predicted by the competitive Langmuir isotherm model. Initial pH:3; T: 20°C.

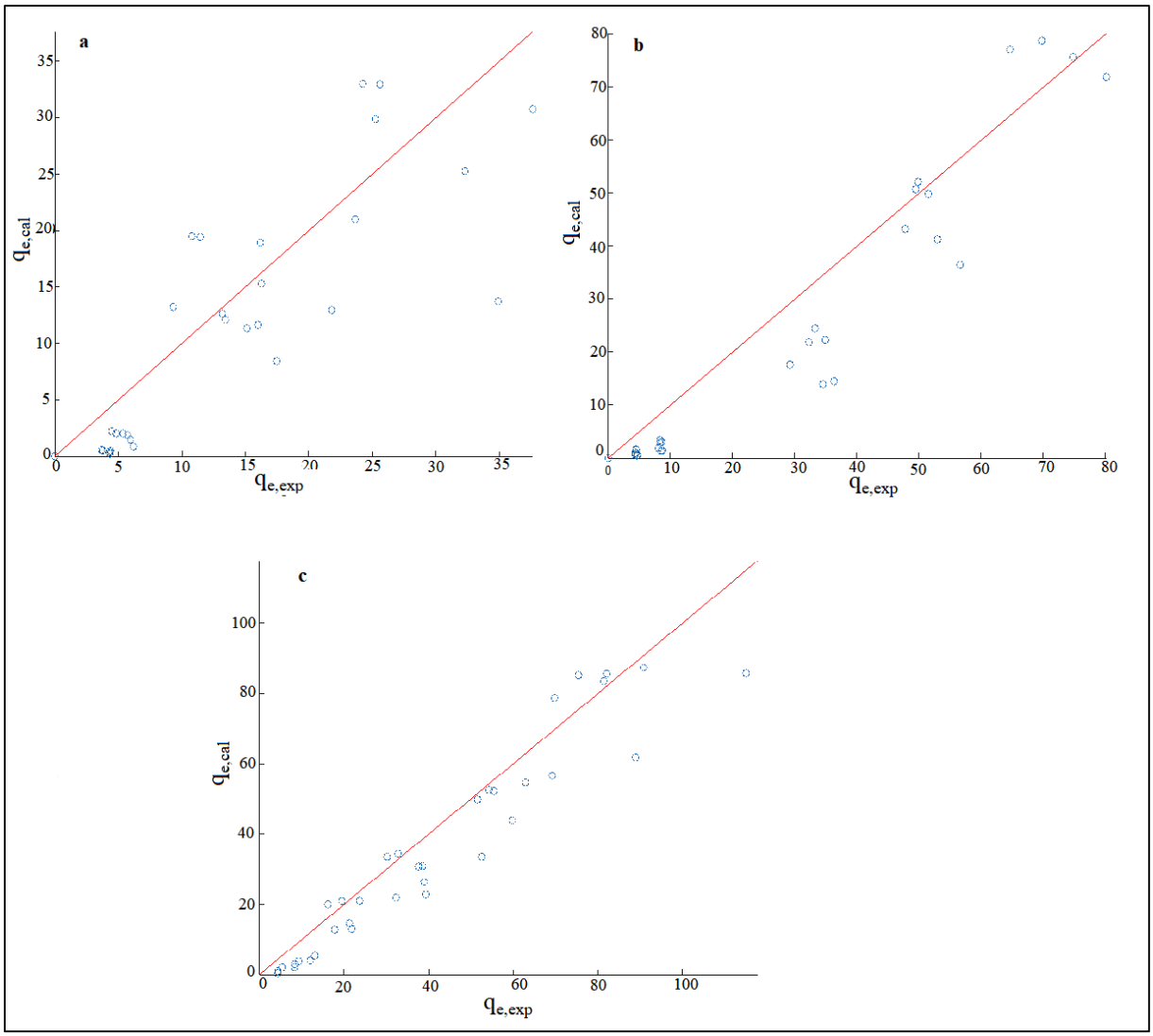

Fig. 10. Calculated versus experimental q_e for the bicomponent system Cr(VI)–Cu(II): (a) Cr(VI), (b) Cu(II) and (c) total metal.

Table 5 Equilibrium isotherm constants of the adsorption of Cu(II) and Cr(VI) ions onto MPCB in binary system.

Isotherm model	**Parameters**	**Metal ions**	
		Cu(II)	**Cr(VI)**
Modified competitive Langmuir	$K_{L,i}$	0.025	0.016
	q_m(mg/beads)	0.015	0.07
	n	29.39	61.78

	SSR	0.44	0.76

3.6 Discussion on the adsorption mechanism of Cu(II) and Cr(VI) onto MPCB

In order to explore the sorption mechanism of Cu(II) and Cr(VI) onto MPCB, SEM, EDX and FTIR analysis were carried out. SEM results showed that the surface morphology of MPCB have changed to smooth and homogenous, indicating that it was covered by Cr(VI) and Cu(II) (Fig.11b and c). These result were confirmed by EDX spectra in which appeared new peaks related to Cr(VI) and Cu(II) after adsorption onto MBCB given in Fig. 11d and e. FTIR spectra of the biocomposite beads (Fig.4) confirmed the presence of hydroxyl, carbonyl and carboxyl groups which could be involved in the adsorption process. FTIR results of MPCB-Cu(II) and MPCB-Cr(VI) were shown in Fig. 12. After Cu adsorption, the characteristic adsorption peak of hydroxyl was redshifted to 3287 cm^{-1} and its intensity has decreased, indicating that these functional groups are highly involved in the adsorption process through surface complexation/chelation [34]. A decrease in the relative intensities with an obvious redshift displacement of the carboxyl group in the Cu loaded spectrum suggested the metal binding with carboxyl groups via electrostatic attraction and surface complexation [44] These results are in good agreement with the results obtained by studying the pH effect. Also, the shift of –OH, –COO and CO adsorption band indicated that ion exchange could be implicated in the adsorption process. Cu(II) ions can be exchanged with the crosslinked calcium in the magnetic pine cones gel beads [80, 85]. This was confirmed by the EDX results. The elemental analysis showed a decrease in calcium percentage from 6.67 to 1.23% after Cu adsorption. The adsorption peak at 533.3 cm^{-1} related to Fe–O was moved to larger wavenumber length, suggesting the possibility of binding with copper ions through Fe–O–Cu

[86]. The FTIR spectra of MPCB-Cr(VI) exhibited peaks at 3348, 2939, 1724, 1599, 1030, 538 cm^{-1} ascribed to –OH, –CH, $–COO^-$, C–O stretching and Fe–O groups. It is noteworthy that the characteristic peaks of hydroxyl and carboxyl have decreased in relative intensities and located to larger wavenumber length (3272 to 3348 cm^{-1}, 1599 to 1724 cm^{-1}), suggesting that these groups contributed in Cr(VI) uptake. Chromium hexavalent species are highly pH depending, at lower pH the MPCB surface functional groups are protonated acquiring positive charges ($–OH_2^+$, $–COOH_2^+$) which favored the electrostatic interaction with the main anionic form of hexavalent chromium $HCrO_4^-$. Furthermore these functional groups act as electron-donor groups which facilitated the reduction of Cr(VI) to Cr(III) with lower toxicity [31, 87].

Cr(III) can gather on MPCB via surface complexation (Eq. (21) and (22)) and ion exchange with Ca^{2+} (Eq. (23)).

$\equiv B–OH + Cr^{3+} \rightarrow \equiv B–OHCr^{3+}$ (21)

$\equiv B–OH_2^+ + HCrO_4^- \rightarrow \equiv B–HCrO_4^- + H_2O$ (22)

$3\ –(COO)_2Ca + 2\ Cr^{3+} \rightarrow 2\ –(COO)_3Cr + 3\ Ca^{2+}$ (23)

The possibility of ion exchange between Ca(II) and Cr(III) was confirmed by the EDX results after Cr(VI) sorption showed a decrease in the percentage of Ca ions. Similar results were reported by Gusmaroli et al [88]. It was reported that the remaining Cr(III) concentration in solution was negligible, indicating its entrapment into the beads [88].

The characteristic peak of Fe–O was redshifted to 537 cm^{-1} and strengthened after the adsorption of Cr(VI) ions, demonstrating the possibility of interaction with Cr(VI) and confirming the possibility of Cr(VI) reduction by Fe(II) in the magnetite given in the pH results [54, 89]. Accordingly, the Cr (VI) sorption mechanism is adsorption-coupled reduction mechanism [87, 90, 91] The FTIR spectra of MPCB loaded Cu(II)/Cr(VI) showed similar characteristic peaks to those of MPCB-Cu(II) and MPCB-Cr.

To sum up the possible mechanism (Fig. 13) of hexavalent chromium and copper (II) sorption might involve electrostatic interaction, surface complexation with functional groups and ion exchange. These finding were in good agreement with the fitting results to the physic model which indicates that the metal ions interacted via one and two functional group but with two different percentages.

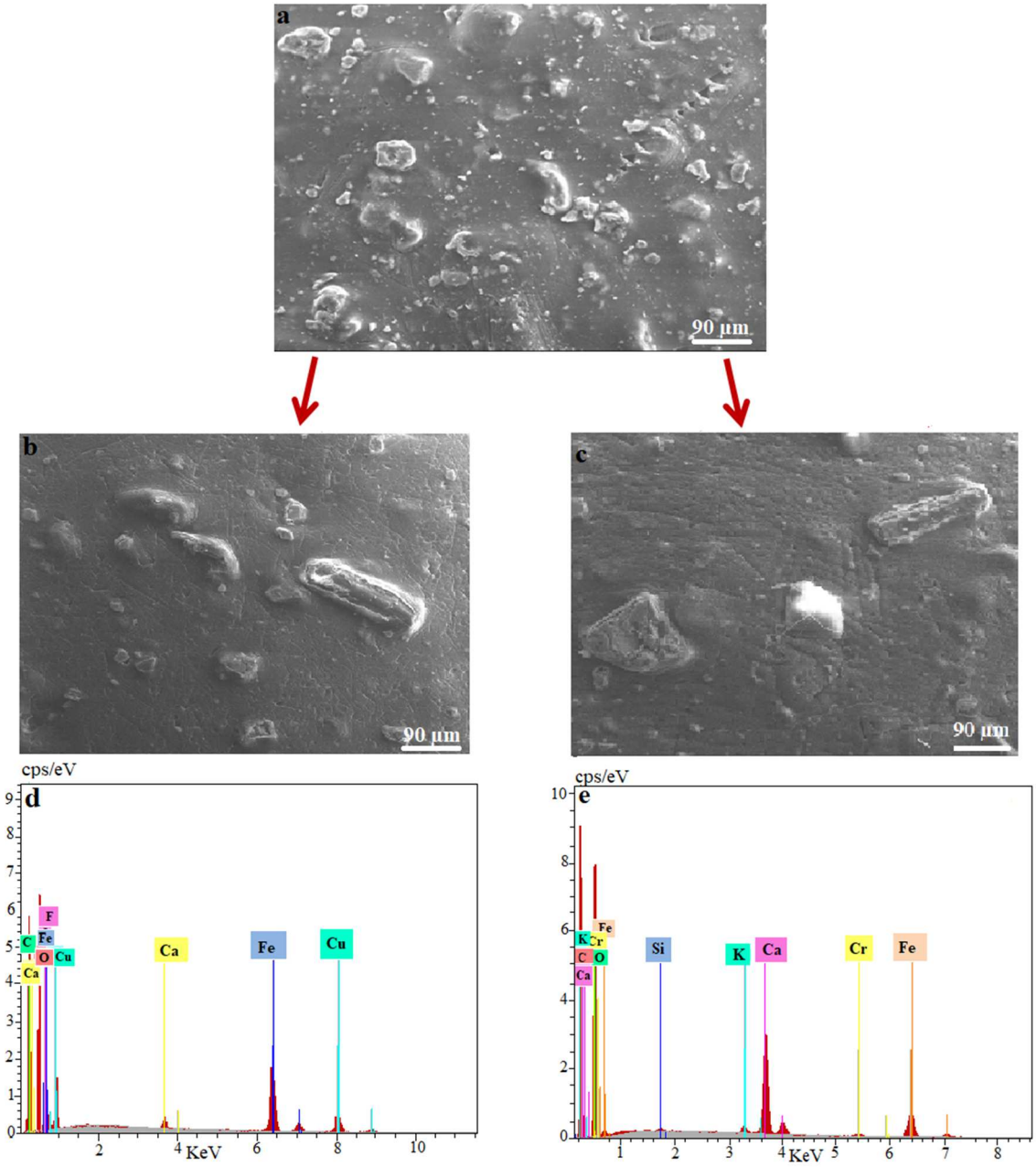

Fig. 11.SEM figures of MPCB: (a) before adsorption, (b) after Cr(VI) sorption, (c) after Cu(II) sorption (magnification: 200 x); EDX spectra of: (d) MPCB-loaded Cr, (e) MPCB-loaded Cu(II).

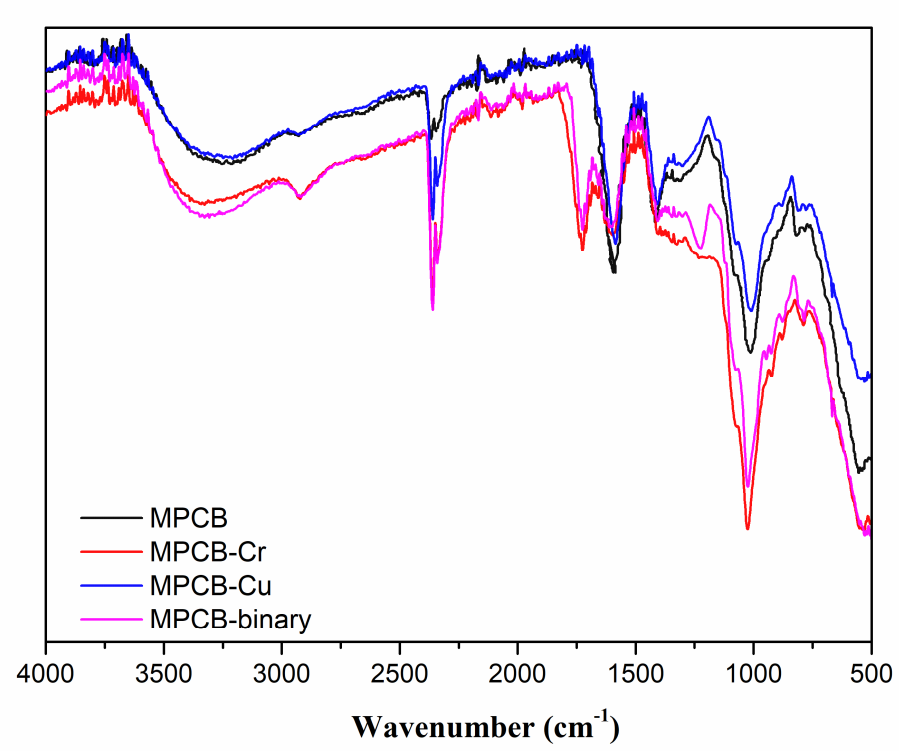

Fig. 12. FTIR spectra of :MPCB before adsorption, MBCB loaded: Cu; Cr; Cu/Cr.

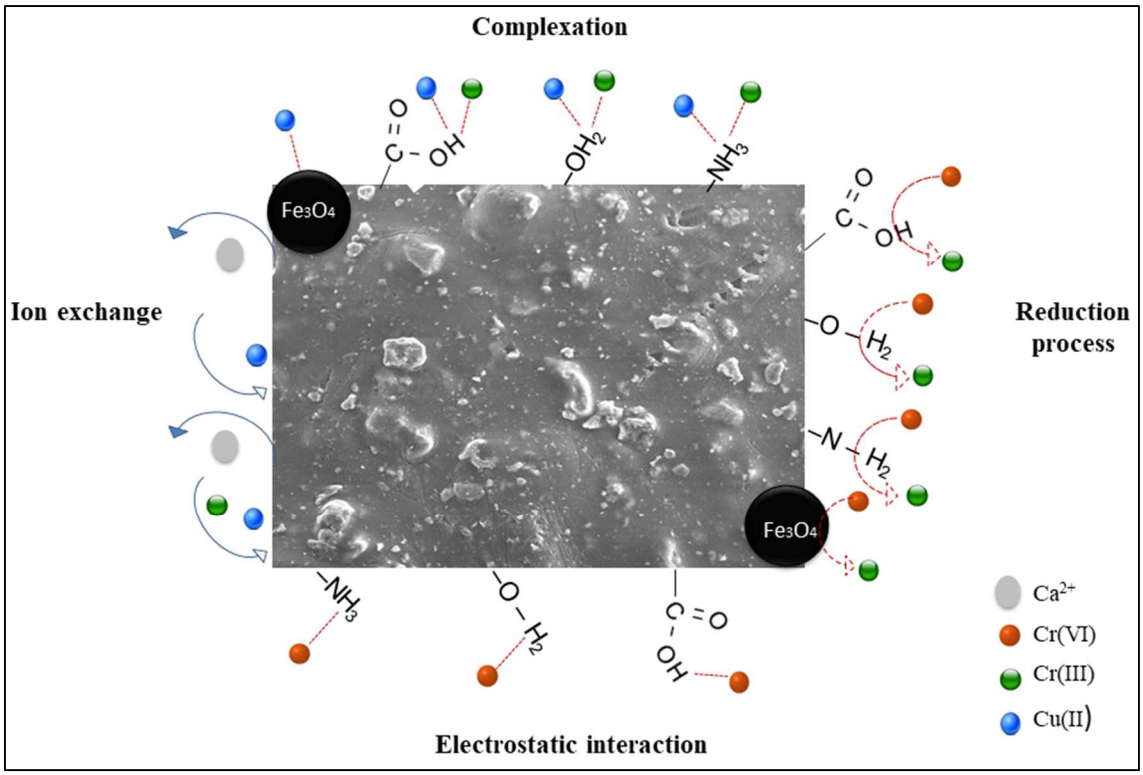

Fig. 13. The adsorption mechanism of Cu(II) and Cr(VI) onto MPCB.

4. Conclusion

In this work, novel biocomposite magnetic pine cones gel beads was successfully synthesized and investigated for Cu(II) and Cr(VI) sorption in single and multi-component mixture. The metal uptake onto MPCB was highly dependent on pH ($pH_{opt/Cu(II)}$: 5; $pH_{opt/Cr}$: 2), initial metal concentration and contact time. The maximum adsorption capacities of Cu (II) and Cr(VI) onto the magnetic biocomposite were 69.77 mg g^{-1} and 132.52 mg g^{-1} respectively. The sorption mechanism was investigated by FTIR and SEM/EDX analysis and the results showed that electrostatic interaction, surface complexation with functional groups and ion exchange were involved in the sorption process. The Langmuir model fitted well the experimental data for both metals, indicating the monolayer sorption. Physical modeling investigation was used to further explain the adsorption mechanism indicating that both ions interacted via one and

two functional group but with different percentages. The pseudo second order model correlates well the kinetic results for both metals confirming the chemisorption mechanism. The competitive effect of metal ion on each other was studied in bicomponent system. The results revealed that the Cr(VI) sorption was inhibited by the presence of Cu(II) indicating the antagonistic effect exerted by Cu(II) ions. Meanwhile, Cu(II) sorption was not influenced by the coexistence of Cr(VI). The binary adsorption data were modeled by the modified competitive Langmuir multi-component isotherm, which showed a good fitting with Cu(II) ions adsorption data. These results suggest that the magnetic pine cones gel beads is a promising sorbent for potentially toxic metals recovery from wastewater.

Acknowledgments

This research was funded by the Spanish Ministry of Science and Innovation as part of the project CTM2015-68859-C2-1-R (MINECO-FEDER).

References

[1] M. Jain, M. Yadav, T. Kohout, M. Lahtinen, V.K. Garg, M.J.W.r. Sillanpää, industry, Development of iron oxide/activated carbon nanoparticle composite for the removal of Cr (VI), Cu (II) and Cd (II) ions from aqueous solution, 20 (2018) 54-74.

[2] A.Q. Selim, L. Sellaoui, S.A. Ahmed, M. Mobarak, E.A. Mohamed, A.B. Lamine, A. Erto, A. Bonilla-Petriciolet, M.K. Seliem, Statistical physics-based analysis of the adsorption of Cu2+ and Zn2+ onto synthetic cancrinite in single-compound and binary systems, Journal of Environmental Chemical Engineering 7 (2019) 103217.

[3] F. Zhang, X. Tang, Y. Huang, A.A. Keller, J. Lan, Competitive removal of Pb2+ and malachite green from water by magnetic phosphate nanocomposites, Water research 150 (2019) 442-451.

[4] W.W. Ngah, M.M.J.B.t. Hanafiah, Removal of heavy metal ions from wastewater by chemically modified plant wastes as adsorbents: a review, 99 (2008) 3935-3948.

[5] C. Barquilha, E. Cossich, C. Tavares, E. Silva, Biosorption of nickel (II) and copper (II) ions by Sargassum sp. in nature and alginate extraction products, Bioresource Technology Reports 5 (2019) 43-50.

[6] B.R. Stern, Essentiality and toxicity in copper health risk assessment: overview, update and regulatory considerations, Journal of Toxicology and Environmental Health, Part A 73 (2010) 114-127.

[7] M. Pohanka, Copper and copper nanoparticles toxicity and their impact on basic functions in the body, Bratisl. Lek. Listy 120 (2019) 397-409.

[8] A. Sinkovič, A. Strdin, F. Svenšek, Severe acute copper sulphate poisoning: a case report, Archives of Industrial Hygiene and Toxicology 59 (2008) 31-35.

[9] A. Zhitkovich, Chromium in drinking water: sources, metabolism, and cancer risks, Chemical research in toxicology 24 (2011) 1617-1629.

[10] I. Aharchaou, J.S. Py, S. Cambier, J.L. Loizeau, G. Cornelis, P. Rousselle, E. Battaglia, D.A. Vignati, Chromium hazard and risk assessment: New insights from a detailed speciation study in a standard test medium, Environmental toxicology and chemistry 37 (2018) 983-992.

[11] B. Chen, J. Xiong, J.-H. Ding, B.-F. Yuan, Y.-Q. Feng, Analysis of the effects of Cr (VI) exposure on mRNA modifications, Chemical research in toxicology 32 (2019) 2078-2085.

[12] J.J. Beaumont, R.M. Sedman, S.D. Reynolds, C.D. Sherman, L.-H. Li, R.A. Howd, M.S. Sandy, L. Zeise, G.V. Alexeeff, Cancer mortality in a Chinese population exposed to hexavalent chromium in drinking water, Epidemiology (2008) 12-23.

[13] J. Barnhart, Occurrences, uses, and properties of chromium, Regulatory toxicology and pharmacology 26 (1997) S3-S7.

[14] K. Yan, Z. Liu, Z. Li, R. Yue, F. Guo, Z. Xu, Selective separation of chromium from sulphuric acid leaching solutions of mixed electroplating sludge using phosphate precipitation, Hydrometallurgy 186 (2019) 42-49.

[15] Y. Al-Degs, M. Khraisheh, M. Tutunji, Sorption of lead ions on diatomite and manganese oxides modified diatomite, Water Research 35 (2001) 3724-3728.

[16] N. Chitpong, S.M. Husson, High-capacity, nanofiber-based ion-exchange membranes for the selective recovery of heavy metals from impaired waters, Separation and Purification Technology 179 (2017) 94-103.

[17] S. Mukherjee, S. Mukhopadhyay, A. Pariatamby, M.A. Hashim, G. Redzwan, B.S. Gupta, Optimization of pulp fibre removal by flotation using colloidal gas aphrons generated from a natural surfactant, Journal of the Taiwan Institute of Chemical Engineers 53 (2015) 15-21.

[18] N. Meunier, P. Drogui, C. Montané, R. Hausler, G. Mercier, J.-F. Blais, Comparison between electrocoagulation and chemical precipitation for metals removal from acidic soil leachate, Journal of hazardous materials 137 (2006) 581-590.

[19] H.E. Reynel-Avila, D.I. Mendoza-Castillo, V. Hernández-Montoya, A. Bonilla-Petriciolet, Multicomponent removal of heavy metals from aqueous solution using low-cost sorbents, Nova Science Publisher, New York, 2011, pp. 69-99.

[20] I. Ali, New generation adsorbents for water treatment, Chemical reviews 112 (2012) 5073-5091.

[21] S. Rangabhashiyam, P. Balasubramanian, Performance of novel biosorbents prepared using native and NaOH treated Peltophorum pterocarpum fruit shells for the removal of malachite green, Bioresource Technology Reports 3 (2018) 75-81.

[22] A. Witek-Krowiak, Analysis of influence of process conditions on kinetics of malachite green biosorption onto beech sawdust, Chemical Engineering Journal 171 (2011) 976-985.

[23] L. Dupont, E. Guillon, Removal of hexavalent chromium with a lignocellulosic substrate extracted from wheat bran, Environmental science & technology 37 (2003) 4235-4241.

[24] T. Ahmad, M. Danish, Prospects of banana waste utilization in wastewater treatment: A review, Journal of environmental management 206 (2018) 330-348.

[25] L. Bulgariu, M. Rățoi, D. Bulgariu, M. Macoveanu, Equilibrium Study of Pb (II) and Hg (II) Sorption from Aqueous Solutions by Moss Peat, Environmental Engineering & Management Journal (EEMJ) 7 (2008).

[26] A.L. Squissato, A.F. Lima, E.S. Almeida, D. Pasquini, E.M. Richter, R.A. Munoz, Eucalyptus pulp as an adsorbent for metal removal from biodiesel, Industrial Crops and Products 95 (2017) 1-5.

[27] W. Tan, S. Ooi, C. Lee, Removal of chromium (VI) from solution by coconut husk and palm pressed fibres, Environmental technology 14 (1993) 277-282.

[28] A.P. Lim, A.Z. Aris, A review on economically adsorbents on heavy metals removal in water and wastewater, Reviews in Environmental Science and Bio/Technology 13 (2014) 163-181.

[29] A. Pholosi, E.B. Naidoo, A.E. Ofomaja, Batch and continuous flow studies of Cr (VI) adsorption from synthetic and real wastewater by magnetic pine cone composite, Chemical Engineering Research and Design 153 (2020) 806-818.

[30] O. Plohl, U. Ajdnik, S. Gyergyek, I. Ban, A. Vesel, T.K. Glaser, L.F. Zemljič, Superior stability and high biosorbent efficiency of carboxymethylchitosan covalently linked to silica-coated core-shell magnetic nanoparticles for application in copper removal, Journal of Environmental Chemical Engineering 7 (2019) 102913.

[31] A. Pholosi, E.B. Naidoo, A.E. Ofomaja, Intraparticle diffusion of Cr (VI) through biomass and magnetite coated biomass: A comparative kinetic and diffusion study, South African Journal of Chemical Engineering 32 (2020) 39-55.

[32] S. Sadeghi, F.A. Rad, A.Z. Moghaddam, A highly selective sorbent for removal of Cr (VI) from aqueous solutions based on Fe3O4/poly (methyl methacrylate) grafted Tragacanth gum nanocomposite: optimization by experimental design, Materials Science and Engineering: C 45 (2014) 136-145.

[33] S. Daneshfozoun, M. Abdullah, B. Abdullah, Preparation and characterization of magnetic biosorbent based on oil palm empty fruit bunch fibers, cellulose and Ceiba pentandra for heavy metal ions removal, Industrial Crops and Products 105 (2017) 93-103.

[34] C. Zhang, S. Liu, S. Li, Y. Tao, P. Wang, X. Ma, L. Chen, Enahanced biosorption of Cu (II) by magnetic chitosan microspheres immobilized Aspergillus sydowii (MCMAs) from aqueous solution, Colloids and Surfaces A: Physicochemical and Engineering Aspects 581 (2019) 123813.

[35] G. Vilardi, J.M. Ochando-Pulido, N. Verdone, M. Stoller, L. Di Palma, On the removal of hexavalent chromium by olive stones coated by iron-based nanoparticles: Equilibrium study and chromium recovery, Journal of cleaner production 190 (2018) 200-210.

[36] J. Kazemi, V. Javanbakht, Alginate beads impregnated with magnetic Chitosan@ Zeolite nanocomposite for cationic methylene blue dye removal from aqueous solution, International journal of biological macromolecules 154 (2020) 1426-1437.

[37] G. Germanos, S. Youssef, W. Farah, B. Lescop, S. Rioual, M. Abboud, The impact of magnetite nanoparticles on the physicochemical and adsorption properties of magnetic alginate beads, Journal of Environmental Chemical Engineering 8 (2020) 104223.

[38] H. Šillerová, M. Komárek, C. Liu, J. Poch, I. Villaescusa, Biosorbent encapsulation in calcium alginate: Effects of process variables on Cr (VI) removal from solutions, International journal of biological macromolecules 80 (2015) 260-270.

[39] H.C. Vu, A.D. Dwivedi, T.T. Le, S.-H. Seo, E.-J. Kim, Y.-S. Chang, Magnetite graphene oxide encapsulated in alginate beads for enhanced adsorption of Cr (VI) and As (V) from

aqueous solutions: role of crosslinking metal cations in pH control, Chemical Engineering Journal 307 (2017) 220-229.

[40] A. Yazidi, L. Sellaoui, M. Badawi, E.C. Lima, A. Bonilla-Petriciolet, P.S. Thue, N.F. Cimirro, A.B. Lamine, Physicochemical interpretation of the adsorption of 4-Bromophenol and 4-Chloroaniline on an activated carbon, Journal of Environmental Chemical Engineering 8 (2020) 104542.

[41] S.-W. Cao, Y.-J. Zhu, Y.-P. Zeng, Formation of γ-Fe2O3 hierarchical nanostructures at 500° C in a high magnetic field, Journal of magnetism and magnetic materials 321 (2009) 3057-3060.

[42] K.G. Raj, P.A. Joy, Coconut shell based activated carbon–iron oxide magnetic nanocomposite for fast and efficient removal of oil spills, Journal of environmental chemical engineering 3 (2015) 2068-2075.

[43] M. Chai, M. Isa, The oleic acid composition effect on the carboxymethyl cellulose based biopolymer electrolyte, (2013).

[44] D. Skrzypczak, A. Witek-Krowiak, A. Dawiec-Liśniewska, D. Podstawczyk, K. Mikula, K. Chojnacka, Immobilization of biosorbent in hydrogel as a new environmentally friendly fertilizer for micronutrients delivery, Journal of Cleaner Production 241 (2019) 118387.

[45] A.M.H. Shadi, M.A. Kamaruddin, N.M. Niza, M.I. Emmanuel, M.S. Hossain, N. Ismail, Efficient treatment of raw leachate using magnetic ore iron oxide nanoparticles Fe_2O_3 as nanoadsorbents, Journal of Water Process Engineering 38 (2020) 101637.

[46] R.-S. Norouzian, M.M. Lakouraj, Preparation and heavy metal ion adsorption behavior of novel supermagnetic nanocomposite based on thiacalix [4] arene and polyaniline: conductivity, isotherm and kinetic study, Synthetic Metals 203 (2015) 135-148.

[47] X. Sun, L. Yang, Q. Li, J. Zhao, X. Li, X. Wang, H. Liu, Amino-functionalized magnetic cellulose nanocomposite as adsorbent for removal of Cr (VI): synthesis and adsorption studies, Chemical Engineering Journal 241 (2014) 175-183.

[48] F. Ahmadpoor, S.A. Shojaosadati, S.Z. Mousavi, Magnetic silica coated iron carbide/alginate beads: Synthesis and application for adsorption of Cu (II) from aqueous solutions, International journal of biological macromolecules 128 (2019) 941-947.

[49] M. Tavana, H. Pahlavanzadeh, M.J. Zarei, The novel usage of dead biomass of green algae of Schizomeris leibleinii for biosorption of copper (II) from aqueous solutions: Equilibrium, kinetics and thermodynamics, Journal of Environmental Chemical Engineering 8 (2020) 104272.

[50] P. Tan, J. Wen, Y. Hu, X. Tan, Adsorption of Cu 2+ and Cd 2+ from aqueous solution by novel electrospun poly (vinyl alcohol)/graphene oxide nanofibers, RSC advances 6 (2016) 79641-79650.

[51] S.S. Baral, S.N. Das, P. Rath, Hexavalent chromium removal from aqueous solution by adsorption on treated sawdust, Biochemical Engineering Journal 31 (2006) 216-222.

[52] M. Akram, H.N. Bhatti, M. Iqbal, S. Noreen, S. Sadaf, Biocomposite efficiency for Cr (VI) adsorption: Kinetic, equilibrium and thermodynamics studies, Journal of Environmental Chemical Engineering 5 (2017) 400-411.

[53] S. Zhu, S. Wang, X. Yang, S. Tufail, C. Chen, X. Wang, J. Shang, Green sustainable and highly efficient hematite nanoparticles modified biochar-clay granular composite for Cr (VI) removal and related mechanism, Journal of Cleaner Production 276 (2020) 123009.

[54] S. Yang, Q. Li, L. Chen, Z. Chen, Z. Pu, H. Wang, S. Yu, B. Hu, J. Chen, X. Wang, Ultrahigh sorption and reduction of Cr (VI) by two novel core-shell composites combined with Fe3O4 and MoS2, Journal of hazardous materials 379 (2019) 120797.

[55] W. Lu, J. Li, Y. Sheng, X. Zhang, J. You, L. Chen, One-pot synthesis of magnetic iron oxide nanoparticle-multiwalled carbon nanotube composites for enhanced removal of Cr (VI) from aqueous solution, Journal of colloid and interface science 505 (2017) 1134-1146.

[56] N.A. Fathy, S.T. El-Wakeel, R.R. Abd El-Latif, Biosorption and desorption studies on chromium (VI) by novel biosorbents of raw rutin and rutin resin, Journal of Environmental Chemical Engineering 3 (2015) 1137-1145.

[57] C. Li, X. Wang, D. Meng, L. Zhou, Facile synthesis of low-cost magnetic biosorbent from peach gum polysaccharide for selective and efficient removal of cationic dyes, International journal of biological macromolecules 107 (2018) 1871-1878.

[58] S.-H. Yu, H. Li, Q.-Z. Yao, S.-Q. Fu, G.-T. Zhou, Microwave-assisted preparation of sepiolite-supported magnetite nanoparticles and their ability to remove low concentrations of Cr (VI), RSC advances 5 (2015) 84471-84482.

[59] S. Lagrergen, Zur Theorie Der Sogenannten Adsorption Gelöster Stoffe Kungliga Svenska Vetenskapsakademiens, Handlingar 24 (1898) 1-39.

[60] Y. Ho, G. McKay, The kinetics of sorption of basic dyes from aqueous solution by sphagnum moss peat, The Canadian Journal of Chemical Engineering 76 (1998) 822-827.

[61] W.J. Weber, J.C. Morris, Kinetics of adsorption on carbon from solution, Journal of the sanitary engineering division 89 (1963) 31-60.

[62] L. Wang, A. Wang, Adsorption characteristics of Congo Red onto the chitosan/montmorillonite nanocomposite, Journal of hazardous materials 147 (2007) 979-985.

[63] Z. Belala, M. Jeguirim, M. Belhachemi, F. Addoun, G. Trouvé, Biosorption of basic dye from aqueous solutions by Date Stones and Palm-Trees Waste: Kinetic, equilibrium and thermodynamic studies, Desalination 271 (2011) 80-87.

[64] H. Annab, N. Fiol, I. Villaescusa, A. Essamri, A proposal for the sustainable treatment and valorisation of olive mill wastes, Journal of Environmental Chemical Engineering 7 (2019) 102803.

[65] M. Wang, L. Xu, J. Peng, M. Zhai, J. Li, G. Wei, Adsorption and desorption of Sr (II) ions in the gels based on polysaccharide derivates, Journal of Hazardous Materials 171 (2009) 820-826.

[66] K.Y. Foo, B.H. Hameed, Insights into the modeling of adsorption isotherm systems, Chemical engineering journal 156 (2010) 2-10.

[67] M.S. Shamsudin, S.F. Azha, L. Sellaoui, M. Badawi, Y.O. Al-Ghamdi, A. Bonilla-Petriciolet, S. Ismail, Fabrication and characterization of a thin coated adsorbent for antibiotic and analgesic adsorption: Experimental investigation and statistical physical modelling, Chemical Engineering Journal 401 (2020) 126007.

[68] T. Altun, H. Ecevit, Cr (VI) removal using Fe 2 O 3-chitosan-cherry kernel shell pyrolytic charcoal composite beads, Environmental Engineering Research 25 (2020) 426-438.

[69] S. Anush, H. Chandan, B. Gayathri, N. Manju, B. Vishalakshi, B. Kalluraya, Graphene oxide functionalized chitosan-magnetite nanocomposite for removal of Cu (II) and Cr (VI) from waste water, International Journal of Biological Macromolecules 164 (2020) 4391-4402.

[70] A. Mittal, R. Ahmad, I. Hasan, Poly (methyl methacrylate)-grafted alginate/Fe3O4 nanocomposite: synthesis and its application for the removal of heavy metal ions, Desalination and Water Treatment 57 (2016) 19820-19833.

[71] Z. Wu, W. Deng, W. Zhou, J. Luo, Novel magnetic polysaccharide/graphene oxide@ Fe3O4 gel beads for adsorbing heavy metal ions, Carbohydrate polymers 216 (2019) 119-128.

[72] K. Vijayalakshmi, T. Gomathi, S. Latha, T. Hajeeth, P. Sudha, Removal of copper (II) from aqueous solution using nanochitosan/sodium alginate/microcrystalline cellulose beads, International journal of biological macromolecules 82 (2016) 440-452.

[73] M. Fatehi, J. Shayegan, M. Zabihi, I. Goodarznia, Functionalized magnetic nanoparticles supported on activated carbon for adsorption of Pb (II) and Cr (VI) ions from saline solutions, Journal of Environmental Chemical Engineering 5 (2017) 1754-1762.

[74] Q.-Q. Zhong, Q.-Y. Yue, B.-Y. Gao, Q. Li, X. Xu, A novel amphoteric adsorbent derived from biomass materials: Synthesis and adsorption for Cu (II)/Cr (VI) in single and binary systems, Chemical engineering journal 229 (2013) 90-98.

[75] D. Pujol, M. Bartrolí, N. Fiol, F. de la Torre, I. Villaescusa, J. Poch, Modelling synergistic sorption of Cr (VI), Cu (II) and Ni (II) onto exhausted coffee wastes from binary mixtures Cr (VI)–Cu (II) and Cr (VI)–Ni (II), Chemical engineering journal 230 (2013) 396-405.

[76] W.E. Marshall, L.H. Wartelle, Chromate (CrO42−) and copper (Cu2+) adsorption by dual-functional ion exchange resins made from agricultural by-products, Water Research 40 (2006) 2541-2548.

[77] K. Rout, M. Mohapatra, S. Anand, A critical analysis of cation adsorption from single and binary solutions on low surface area β-MnO2, Applied surface science 270 (2013) 205-218.

[78] X. Sun, H. Huang, Y. Zhu, Y. Du, L. Yao, X. Jiang, P. Gao, Adsorption of Pb2+ and Cd2+ onto Spirulina platensis harvested by polyacrylamide in single and binary solution systems, Colloids and Surfaces A: Physicochemical and Engineering Aspects 583 (2019) 123926.

[79] B. Agarwal, P. Thakur, C. Balomajumder, Use of iron-impregnated granular activated carbon for co-adsorptive removal of phenol and cyanide: Insight into equilibrium and kinetics, Chemical Engineering Communications 200 (2013) 1278-1292.

[80] D. Park, Y.-S. Yun, K.H. Yim, J.M. Park, Effect of Ni (II) on the reduction of Cr (VI) by Ecklonia biomass, Bioresource technology 97 (2006) 1592-1598.

[81] C. Zhu, F. Liu, Y. Zhang, M. Wei, X. Zhang, C. Ling, A. Li, Nitrogen-doped chitosan-Fe (III) composite as a dual-functional material for synergistically enhanced co-removal of Cu (II) and Cr (VI) based on adsorption and redox, Chemical Engineering Journal 306 (2016) 579-587.

[82] Z. Yu, W. Song, J. Li, Q. Li, Improved simultaneous adsorption of Cu (II) and Cr (VI) of organic modified metakaolin-based geopolymer, Arabian Journal of Chemistry 13 (2020) 4811-4823.

[83] H.E. Reynel-Avila, D.I. Mendoza-Castillo, A.A. Olumide, A. Bonilla-Petriciolet, A survey of multi-component sorption models for the competitive removal of heavy metal ions using bush mango and flamboyant biomasses, Journal of Molecular Liquids 224 (2016) 1041-1054.

[84] J.B. Neris, F.H.M. Luzardo, E.G.P. da Silva, F.G. Velasco, Evaluation of adsorption processes of metal ions in multi-element aqueous systems by lignocellulosic adsorbents applying different isotherms: a critical review, Chemical Engineering Journal 357 (2019) 404-420.

[85] H. Ding, X. Zhang, H. Yang, X. Luo, X. Lin, Highly efficient extraction of thorium from aqueous solution by fungal mycelium-based microspheres fabricated via immobilization, Chemical Engineering Journal 368 (2019) 37-50.

[86] M. Zhu, L. Zhu, J. Wang, T. Yue, R. Li, Z. Li, Adsorption of Cd (II) and Pb (II) by in situ oxidized Fe3O4 membrane grafted on 316L porous stainless steel filter tube and its potential application for drinking water treatment, Journal of environmental management 196 (2017) 127-136.

[87] E.A. Mohamed, A.Q. Selim, S.A. Ahmed, L. Sellaoui, A. Bonilla-Petriciolet, A. Erto, Z. Li, Y. Li, M.K. Seliem, H2O2-activated anthracite impregnated with chitosan as a novel

composite for Cr (VI) and methyl orange adsorption in single-compound and binary systems: Modeling and mechanism interpretation, Chemical Engineering Journal 380 (2020) 122445.

[88] L. Gusmaroli, C. Liu, J. Poch, N. Fiol, G. Alberti, I. Villaescusa, A fast and easy approach to the simulation of binary mixtures sorption kinetics, Science of The Total Environment 616 (2018) 948-959.

[89] F. Pinakidou, M. Katsikini, K. Simeonidis, E. Kaprara, E. Paloura, M. Mitrakas, On the passivation mechanism of Fe3O4 nanoparticles during Cr (VI) removal from water: A XAFS study, Applied Surface Science 360 (2016) 1080-1086.

[90] Y. Chen, D. An, S. Sun, J. Gao, L. Qian, Reduction and removal of chromium VI in water by powdered activated carbon, Materials 11 (2018) 269.

[91] A.T. Vo, V.P. Nguyen, A. Ouakouak, A. Nieva, B.T. Doma, H.N. Tran, H.-P. Chao, Efficient removal of Cr (VI) from water by biochar and activated carbon prepared through hydrothermal carbonization and pyrolysis: adsorption-coupled reduction mechanism, Water 11 (2019) 1164.

Single and Simultaneous adsorption of Cr(VI) and Cu (II) on a novel Fe_3O_4/pine cones gel beads nanocomposite : Experiments, Characterization and isotherms modeling

Manel Touihri[1,*], Fatma Guesmi[1], Chiraz Hannachi[1], Béchir Hamrouni[1], Lotfi Sellaoui[2], Michael Badawi[3,*], Jordi Poch[4], Núria Fiol[5,*]

[1]Laboratory of desalination and water treatment LR19ES01, Faculty of Sciences of Tunis, University of Tunis EL Manar, 2092, Tunis, Tunisia.

[2]Laboratory of Quantum and Statistical Physics, LR18ES18, Monastir University, Faculty of Sciences of Monastir, Tunisia

[3]Laboratoire de Physique et Chimie Théoriques LPCT UMR CNRS 7019, Université de Lorraine, Vandœuvre-lès-Nancy, France

[4]Applied Informatics and Mathematics Department. Universitat de Girona. Campus Montilivi, 17003, Girona, Spain.

[5]ChemicalEngineering Department. Universitat de Girona. Campus Montilivi, 17003, Girona, Spain.

Corresponding authors: [*]Manel Touihri, manel.touihri@fst.utm.tn

[*]Michael Badawi, michael.badawi@univ-lorraine.fr

[*]Núria Fiol, nuria.fiol@udg.edu

Graphical abstract